Domain structure of bulk ferromagnetic crystals in applied fields near saturation

Hans Knüpfer * Cyrill B. Muratov †

April 27, 2010

Abstract

We investigate the ground state of a uniaxial ferromagnetic plate with perpendicular easy axis and subject to an applied magnetic field normal to the plate. Our interest is the asymptotic behavior of the energy in macroscopically large samples near the saturation field. We establish the scaling of the critical value of the applied field strength below saturation at which the ground state changes from the uniform to a branched domain magnetization pattern and the leading order scaling behavior of the minimal energy. Furthermore, we derive a reduced sharp-interface energy giving the precise asymptotic behavior of the minimal energy in macroscopically large plates under a physically reasonable assumption of small deviations of the magnetization from the easy axis away from domain walls. On the basis of the reduced energy, and by a formal asymptotic analysis near the transition, we derive the precise asymptotic values of the critical field strength at which non-trivial minimizers (either local or global) emerge. The non-trivial minimal energy scaling is achieved by magnetization patterns consisting of long slender needle-like domains of magnetization opposing the applied field.

Contents

*Courant Institute of Mathematical Sciences, New York University, New York, NY 10012
†Department of Mathematical Sciences, New Jersey Institute of Technology, Newark, NJ 07102

1 Introduction

Ferromagnetic materials offer a fascinating example of physical systems capable of producing an extraordinarily rich variety of spatial patterns [16]. By a pattern in a ferromagnet, one usually understands a stable spatial distribution of the magnetization vector in the sample. This definition reflects the mesoscopic nature of the magnetization patterns: they are observed on the length scales significantly exceeding the atomic scale (making the definition of the magnetization per unit volume meaningful), yet they are susceptible to small random fluctuations due to thermal noise, with the noise providing a selection mechanism for observable patterns.

On the mesoscopic level, the theory describing the spatio-temporal dynamics of the magnetization patterns in ferromagnetic materials is formulated in terms of partial differential equations (with a possible addition of stochastic forcing [2]) for the magnetization vector $\mathbf{M} = \mathbf{M}(\mathbf{r}, t)$ [16,23,25]. At the center of the theory is the micromagnetic energy functional $\mathcal{E}[\mathbf{M}]$ describing the contributions of different physical interactions (for specifics, see the following section) [11,16,19]. Magnetization patterns are viewed as global or, more generally, local minimizers of $\mathcal{E}$, forming mainly due to the competition of the exchange, anisotropy, and the magnetostatic interactions, with the applied external field playing a significant role [16,23]. Because of the non-local nature of the magnetostatic forces, their effect can depend significantly on the geometry of the ferromagnetic sample [11,12,16, 19].

In bulk crystalline materials the local anisotropy energy and the short-ranged exchange energy act jointly to favor magnetization distributions in the form of extended *magnetic domains* in which the magnetization vector stays nearly constant, separated by *domain walls*, where the magnetization direction changes abruptly. It was already realized in the pioneering works of Landau and Lifshitz [24] and Kittel [18] that, while the structure of the domain walls may not be significantly affected by the long-range magnetostatic forces, these forces should determine the relative spatial arrangement of the domains with different orientation of the magnetization. In fact, since the total magnetostatic energy scales faster than volume as the size of the system increases, in large samples the effect of long-range magnetostatic interactions becomes dominant. As a result, the magnetization patterns develop rapid oscillations to cancel out the induced magnetic field and form intricate structures, which are generally referred to as *branched domains*, even though the actual topological branching of the domains is not really required.

Despite a long history of observations of branched domain structures in ferromagnetic materials [16] and related systems (see e.g. [23,29–32]), mathematical understanding of the branching phenomenon started to emerge only recently with the ansatz-free analysis of energy minimizing structures [5, 7] (there is, of course, an extensive literature of ansatz-based studies, see e.g. [15,17,28]). In particular, for bulk crystalline ferromagnets in the absence of an applied field the first rigorous analysis of the branched domain structures was performed in the work of Choksi and Kohn [6]. They studied a sharp interface version of the micromagnetic energy and were able to obtain matching (in the sense of scaling with the sample thickness) upper and lower bounds for the energy of minimizers of the reduced energy. We note that the connection of the sharp interface energy to the full

micromagnetic energy in the limit of high anisotropy was recently established in [27]. The results of [7] are suggestive that the energy minimizers of the sharp interface micromagnetic energy are in some sense not very different from the branched domain ansatz used as a trial function in the calculation of the upper bound of the energy of the minimizers. The latter shares many common features with the branched domain structures observed in experiments [16]. Since then, similar results have also been obtained for models describing type-I superconductors in the intermediate state [5, 8] and diblock-copolymers undergoing microphase separation [4, 9, 26].

Note that the presence of a moderate applied magnetic field does not alter the situation qualitatively. On the other hand, if a very strong external magnetic field is applied to the sample, then it will obviously overwhelm all other effects and result in a uniform magnetization pattern in the direction of the applied field. It is then clear that a bifurcation from the uniform to a non-uniform magnetization pattern will occur when the field strength is gradually reduced. Let us point out that this transition would typically occur via nucleation and growth of new domains and is, therefore, accompanied by a hysteresis. In other words, in a certain range of applied fields one should find coexistence of different types of patterns. Their relative stability and the transition pathways between them are, therefore, important questions to be addressed. Note that these questions also naturally arise in various other problems of energy driven pattern formation, such as type-I and type-II superconductors and Ginzburg-Landau models with Coulomb repulsion [1, 5, 8, 26].

Main results

We investigate the properties of the magnetization patterns in bulk uniaxial crystalline ferromagnets in the presence of external magnetic field applied along the material's easy axis. We are interested in the transition to non-trivial energy minimizers occurring near the saturation field in ferromagnetic plates with perpendicular easy axis.

In Section 3, we establish the scaling behavior of the minimal energy in dependence of the plate thickness and the exterior field. The precise result is stated in Theorems 3.1 and 3.2. As a consequence, we get that in macroscopically large plates the transition from the monodomain to the branched magnetization pattern occurs when the strength H_{ext} of the applied field H_{ext} satisfies

$$H_s - H_{\text{ext}} \;\sim\; \left\{ \frac{AK^2}{L^2 M_s (K + 4\pi M_s^2)} \ln\left(\frac{4\pi^2 L^2 M_s^4}{AK} \right) \right\}^{\frac{1}{3}}, \tag{1.1}$$

where $H_s = 4\pi M_s$ is the saturation field. We refer to Section 2 for the precise definitions of the physical parameters in (1.1). For smaller applied fields the energy of the minimizers per unit area in macroscopically large plates is

$$\frac{\text{Energy}}{\text{Area}} \;\sim\; \left\{ \frac{LAK^2 M_s^2}{K + 4\pi M_s^2} \left(1 - \frac{H_{\text{ext}}}{H_s} \right)^3 \ln\left(1 - \frac{H_{\text{ext}}}{H_s} \right)^{-1} \right\}^{\frac{1}{3}}. \tag{1.2}$$

In particular, the energy per unit area of the plate scales as $L^{\frac{1}{3}}$ with the plate thickness and linearly (up to a slow logarithmic dependence) with the deviation of the applied field from the saturation field. This energy is achieved by trial functions consisting of periodic patterns of slender needle-like disconnected domains of magnetization opposing the applied field. In each unit cell of such a trial function the magnetization pattern refines toward the plate boundaries in a self-similar fashion (see

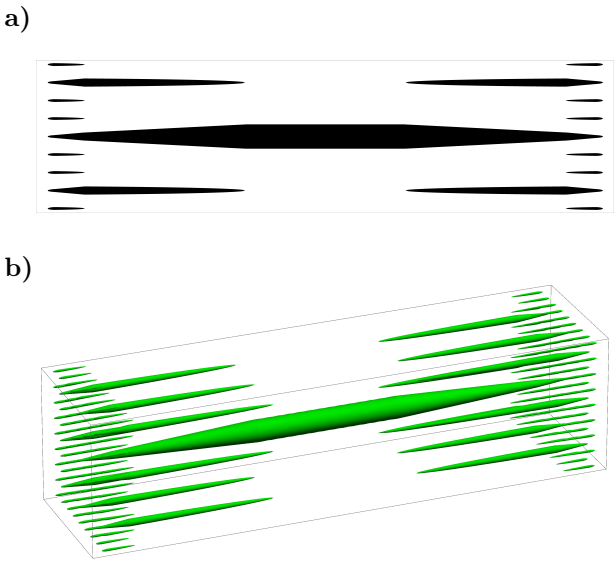

Figure 1: A sketch of the refining needle configuration. (a) The projection of one period of the domain pattern on the x_1x_2-plane. (b) A three-dimensional sketch of one period of the domain pattern. Shaded regions indicate the domains of magnetization opposing the applied field.

Fig. 1). This class of magnetization patterns is, therefore, a natural candidate for the precise form of the energy minimizers (see also Fig. 2).

In Section 4, we further investigate the asymptotic behavior of the energy in macroscopic samples. Under a physically reasonable assumption that the magnetization vector does not deviate strongly from the easy axis, we rigorously derive a reduced energy, whose minimum agrees asymptotically with the sharp interface version of the energy, see Theorem 4.1. The obtained result assigns a mathematical meaning to the μ^*-method for computing the energy contributions away from the domain walls in a magnetization pattern, which was proposed more than half a century ago in the physics literature [33]. The obtained reduced energy, given by (4.2), practically coincides with that of an infinitely hard material in which the strength of magnetostatic interaction has been suitably renormalized. The latter explains why the behavior of minimal energy in both hard and soft materials is the same up to a certain factor in the macroscopic limit. Let us also note that for the same reason the energy per unit area becomes essentially independent of the saturation magnetization M_s in soft materials with fixed value of H_{ext}/H_s, see (1.2).

In Section 5, we perform a formal asymptotic analysis of the reduced energy in (4.2) and establish a precise asymptotic behavior of the critical field H_{c_0} at which the only minimizer (global or local) is expected to be the uniform state, and the critical field H_{c_1} at which non-trivial minimizers emerge, see Theorem 5.1. It turns out that asymptotically for macroscopically large plates

$$1-\frac{H_{c_{0,1}}}{H_s} \;\simeq\; C_{0,1}\left\{\frac{AK^2}{L^2M_s^4(K+4\pi M_s^2)}\ln\left(\frac{4\pi^2L^2M_s^4}{AK}\right)\right\}^{\frac{1}{3}}, \tag{1.3}$$

where $C_0 \approx 0.4368$ and $C_1 \approx 0.5403$. At $H \sim H_{c_{0,1}}$ the magnetization patterns are expected

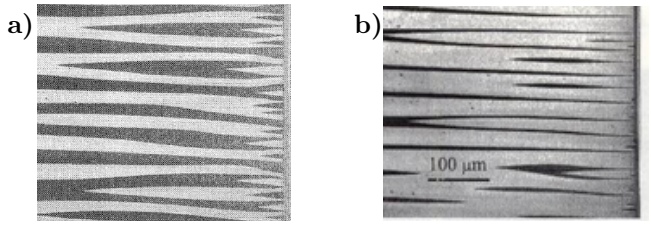

Figure 2: Side views of magnetization domain patterns refining towards the boundary in bulk cobalt crystals: in the absence of the magnetic field (a) and in the applied field at 60% to saturation (b). From Ref. [16].

to consist of slender, approximately radially-symmetric needle-like domains spanning the entire plate thickness and separated by large distances compared to the needle radius. Equation (1.3) is obtained from a reduced one-dimensional expression for the energy of needles, see (5.4). Solving the respective Euler-Lagrange equation exactly, we obtain the precise shape of the needle and, correspondingly, the expression in (1.3).

Structure of the paper and notations

The paper is structured as follows: In Section 2, we present the micromagnetic energy functional and introduce its sharp interface version. In Section 3, we prove matching upper and lower bounds for bulk samples near the critical field. In Section 4, we derive a reduced model that captures the leading order energy in the macroscopic limit. In Section 5, we perform a further reduction of the energy and find the precise location of the transition to non-trivial minimizers by solving the reduced minimization problem exactly.

We will denote a generic point in space by $x = (x_1, x_2, x_3) = (x_1, x_\perp)$, where x_1 is the component in the direction of the easy axis and $x_\perp = (x_2, x_3)$ is the component projection onto the plane normal to the easy axis. Similarly, we will denote the component of a vector $\mathbf{v} \in \mathbb{R}^3$ in the direction of the easy axis by v_1 and its projection to the plane normal to the easy axis by $\mathbf{v}_\perp = (v_2, v_3)$. The spatial gradient is similarly separated into the components along and perpendicular to the easy axis: $\nabla = (\partial_1, \nabla_\perp)$.

We use the symbols $\sim, \lesssim$ and $\gtrsim$ to indicate that an estimate holds up to a universal constant. For example $A \sim B$ means that there are universal constants $c, C > 0$ such that $cA \leq B \leq CA$. The symbols $\ll$ and $\gg$ indicate that an estimate requires a small universal constant. For example, if we say that $A \lesssim B$ for $\varepsilon \ll 1$, this is a short way of saying that $A \leq CB$ holds for all $\varepsilon \leq \varepsilon_0$ where $\varepsilon_0 > 0$ is a small universal constant. By the symbol $\simeq$, we indicate asymptotic equivalence of two expressions: E.g. by writing $A \simeq B$ for $\varepsilon \ll 1$ and $\lambda \ll 1$, we mean that for every $\delta > 0$, there are $\varepsilon_0, \lambda_0 > 0$ such that $|A/B - 1| \leq \delta$ for all $\varepsilon < \varepsilon_0$ and all $\lambda < \lambda_0$.

2 Physical model and sharp interface energy

Micromagnetic energy: Up to an additive constant, the micromagnetic energy for a mono-crystalline

uniaxial ferromagnet (see e.g. [16], using CGS units) is given by

$$\begin{aligned}\mathcal{E}[\mathbf{M}] = \int_{\widetilde{\Omega}} \Big(\frac{A}{2M_s^2} |\nabla \mathbf{M}|^2 + \frac{K}{2M_s^2} |\mathbf{M}_\perp|^2 - \mathbf{H}_{\text{ext}} \cdot \mathbf{M} \Big) \, d^3 r \\ + \frac{1}{2} \int_{\mathbb{R}^3} \int_{\mathbb{R}^3} \frac{\nabla \cdot \mathbf{M}(\mathbf{r}) \, \nabla \cdot \mathbf{M}(\mathbf{r}')}{|\mathbf{r} - \mathbf{r}'|} \, d^3 r \, d^3 r' + \frac{1}{8\pi} \int_{\widetilde{\Omega}} |\mathbf{H}_{\text{ext}}|^2 \, d^3 r\end{aligned} \tag{2.1}$$

Here, $\widetilde{\Omega} \subset \mathbb{R}^3$ describes the region of space occupied by the ferromagnetic material, and the magnetization vector $\mathbf{M} : \mathbb{R}^3 \to \mathbb{R}^3$ satisfies $|\mathbf{M}| = M_s$ in $\widetilde{\Omega}$ and $\mathbf{M} = 0$ outside. The terms in the energy, as they appear in the formula, are:

1. The *exchange* energy favoring a uniform magnetization.
2. The *anisotropy* energy favoring alignment of the magnetization with the easy axis.
3. The *Zeeman* energy favoring alignment with the external field $\mathbf{H}_{\text{ext}}$.
4. The *stray field* energy describing long-range Coulomb interactions of the "magnetic charges" $\nabla \cdot \mathbf{M}$.
5. A *constant* term, added for convenience.

Also in (2.1), A is the exchange constant, M_s is the saturation magnetization and K is the uniaxial anisotropy constant. The subscript "$\perp$" denotes the components of a vector in the plane normal to the easy axis.

Geometry of the sample: We consider a plate of constant thickness L, whose surfaces are oriented in the direction normal to the easy axis. To simplify the issues associated with the treatment of the lateral boundaries of the sample, we assume periodicity with period $\mathcal{L}$ in the plane normal to the easy axis. We hence write $\widetilde{\Omega} = (0, L) \times \widetilde{\mathrm{T}}$, where $\widetilde{\mathrm{T}} = [0, \mathcal{L})^2$ is a torus with periodicity $\mathcal{L}$. The periodicity assumption, however, is not essential, as long as the energy of the minimizers is extensive in $\mathcal{L}$, i.e. we have $\inf \mathcal{E} = O(\mathcal{L}^2)$ as $\mathcal{L} \to \infty$. As we will show below, this will indeed be the case. Also, the external field is assumed to be in the direction of the easy axis (and hence also normal to the material surface):

$$\mathbf{H}_{\text{ext}} = H_{\text{ext}} \, \mathbf{e}_1,$$

where $\mathbf{e}_1$ is the unit vector in the direction of the easy axis.

Rescaling: As usual, we first introduce the exchange length $l_{\text{ex}} = \sqrt{A/(4\pi M_s^2)}$ and the dimensionless quality factor $Q = K/(4\pi M_s^2)$ [16]. Introducing $\mathbf{m} = \mathbf{M}/M_s$, $\mathbf{h}_{\text{ext}} = \mathbf{H}_{\text{ext}}/(4\pi M_s)$, $\ell = \mathcal{L}/L$, and measuring lengths and energy in units of L and $2\pi M_s^2 L^3$, respectively, we can then rewrite (2.1) as

$$\mathcal{E}[\mathbf{m}] = \int_\Omega \frac{l_{\text{ex}}^2}{L^2} |\nabla \mathbf{m}|^2 + Q \int_\Omega |\mathbf{m}_\perp|^2 - \int_\Omega \left(2\mathbf{h}_{\text{ext}} \cdot \mathbf{m} - \mathbf{h} \cdot \mathbf{m} + h_{\text{ext}}^2 \right), \tag{2.2}$$

where $\Omega = (0, 1) \times \mathrm{T}$ is the rescaling of $\widetilde{\Omega}$, with $\mathrm{T} = [0, \ell)^2$, and $|\mathbf{m}| = \chi_\Omega$, where χ_Ω denotes the characteristic function of Ω. The dimensionless stray field $\mathbf{h}$ is defined as the unique (see e.g. [6]) solution in $L^2(\mathbb{R} \times \mathrm{T}; \mathbb{R}^3)$ of

$$\nabla \times \mathbf{h} = 0, \qquad \nabla \cdot \mathbf{h} = -\nabla \cdot \mathbf{m} \qquad \text{in} \quad \mathbb{R} \times \mathrm{T}, \tag{2.3}$$

where (2.3) is understood in the distributional sense.

Sharp interface energy: In a bulk uniaxial material, the magnetization is expected to lie mostly in the direction of the easy axis, i.e. $\mathbf{m} \approx \pm\mathbf{e}_1$. The regions with different orientations of the magnetization are expected to be separated by thin Bloch walls [16, p. 215]. A Bloch wall is characterized by a transition layer of thickness $w \approx Q^{-\frac{1}{2}} l_{\text{ex}}$ in which the magnetization rotates in the wall plane, thus avoiding the creation of a stray field. Taking advantage of the observation in [19, p. 367], one can directly estimate the anisotropy and exchange terms in the energy from below for any $\delta \geq 0$ fixed as

$$\int_{|\mathbf{m}_\perp| \geq \delta} \left(\frac{l_{\text{ex}}^2}{L^2} |\nabla \mathbf{m}|^2 + Q |\mathbf{m}_\perp|^2 \right) \geq \ \varepsilon \int_{|\mathbf{m}_\perp| \geq \delta} |\nabla m_1|, \tag{2.4}$$

with the notation $\mathbf{m} = m_1 \mathbf{e}_1 + \mathbf{m}_\perp$ and where we have introduced

$$\varepsilon = \frac{2 l_{\text{ex}} \sqrt{Q}}{L}. \tag{2.5}$$

In fact, the one-dimensional Bloch wall profile attains equality in (2.4) (see [16]), which implies that the term in the right-hand side of (2.4) should actually well approximate the term in the left-hand side for the energy minimizers. The condition of validity of this approximation is that the wall thickness w remains much smaller than the characteristic length scale of the magnetization pattern. In particular, one should have $w \ll L$. This condition is achieved for sufficiently thick plates. In fact, large thickness is also a necessary condition for branched domain patterns to be observed in ferromagnetic materials [16]. Therefore, in the present context one is naturally interested in the asymptotic behavior of energy for large values of L or, equivalently, in the limit $\varepsilon \to 0$ with all other dimensionless parameters fixed.

Dropping the gradient term in (2.2) where $|\mathbf{m}_\perp| < \delta$ and combining it with (2.4), one can see that

$$\mathcal{E}[\mathbf{m}] \geq \ \varepsilon \int_{|\mathbf{m}_\perp| \geq \delta} |\nabla m_1| \ + Q \int_{|\mathbf{m}_\perp| < \delta} |\mathbf{m}_\perp|^2 - \int_\Omega \left(2\mathbf{h}_{\text{ext}} \cdot \mathbf{m} + \mathbf{h} \cdot \mathbf{m} - h_{\text{ext}}^2 \right). \tag{2.6}$$

This motivates the introduction of a sharp interface energy, in which the gradient-squared term in (2.2) is replaced by the total variation of m_1 (see also [6, 7]). We note, however, that the sharp interface energy is basically a tool to approximate the behavior of the full physical energy in (2.2) and, therefore, can be tailored to our advantage. We choose the sharp interface energy in the form

$$E[\mathbf{m}] = \varepsilon \int_\Omega |\nabla m_1^\delta| + Q \int_{\{|\mathbf{m}_\perp| < \delta\}} |\mathbf{m}_\perp|^2 + \delta^2 Q \int_{\{|\mathbf{m}_\perp| \geq \delta\}} |\mathbf{m}_\perp|^2 - \int_\Omega \left(2\mathbf{h}_{\text{ext}} \cdot \mathbf{m} + \mathbf{h} \cdot \mathbf{m} - h_{\text{ext}}^2 \right). \tag{2.7}$$

Here $0 < \delta \ll 1$ is an arbitrary "cutoff" parameter, whose precise value is inessential (hence the index δ is dropped from the definition of E), and m_1^δ is the truncated version of m_1:

$$m_1^\delta(x) = \begin{cases} 1 - \delta^2, & m_1(x) > 1 - \delta^2, \\ m_1(x), & -1 + \delta^2 \leq m_1(x) \leq 1 - \delta^2, \\ -1 + \delta^2, & m_1(x) < -1 + \delta^2. \end{cases} \tag{2.8}$$

The advantage of using m_1^δ in (2.7) instead of m_1 is that, consistently with (2.6), the interfacial term does not contribute to the energy away from the domain walls, where $m_1 \approx \pm 1$. Importantly, E provides an ansatz-free lower bound for $\mathcal{E}$:

$$\mathcal{E}[\mathbf{m}] \geq (1-\delta^2)E[\mathbf{m}], \tag{2.9}$$

which can be easily seen by retracing the arguments leading to (2.6). Furthermore, since in the limit $\varepsilon \to 0$ the transition regions between different directions of $\mathbf{m}$ are expected to become $O(\varepsilon Q^{-1})$ thin and the inequality in (2.6) to become an equality for minimizers, in view of arbitrariness of δ one should expect that $\inf \mathcal{E} \simeq \inf E$ for $\varepsilon \ll 1$. In the following, we will prove that this relation holds in the sense of scaling, i.e., for sufficiently small $\varepsilon > 0$, we have $\inf \mathcal{E} \sim \inf E$.

Critical external fields: Clearly, when the applied field h_{ext} is sufficiently large, the minimal energy configuration will be such that all magnetic moments are aligned with the field, i.e. $\mathbf{m} = \mathbf{e}_1 \chi_\Omega$. For smaller external fields, the minimizer is attained by other configurations. The external field strength, at which the uniform magnetization $\mathbf{m} = \mathbf{e}_1 \chi_\Omega$ looses its optimality is denoted by h_{c_1}. Let us also note that appearance and disappearance of patterns as a function of the control parameter in systems of this kind is often accompanied by a hysteresis. Therefore, non-trivial critical points of the energy may persist even for fields larger than h_{c_1}. The critical field at which these critical points disappear will be denoted by h_{c_0}.

The saturation field h_s is defined similarly in terms of the *relaxed energy*. In our setting, it is the variant of $\mathcal{E}$ where the surface energy is not penalized, i.e.

$$\mathcal{E}_{\text{rel}}[\mathbf{m}] = \int_\Omega Q|\mathbf{m}_\perp|^2 - \int_\Omega \left(2\mathbf{h}_{\text{ext}} \cdot \mathbf{m} - \mathbf{h} \cdot \mathbf{m} + h_{\text{ext}}^2\right).$$

The set of admissible functions for $\mathcal{E}_{\text{rel}}$ is given by all $\mathbf{m}$ satisfying $|\mathbf{m}| \leq 1$ in Ω. This relaxed constraint in the above calculation can be justified by looking at small-scale oscillations of $\mathbf{m}$. It is related to the fact that $\mathcal{E}_{\text{rel}}$ is non-convex, see e.g. [10, 21]. One expects that the relaxed energy gives the leading order behavior of the minimal energy, i.e.

$$\lim_{\varepsilon \to 0} \inf_{|\mathbf{m}|=1} \mathcal{E}[\mathbf{m}] \;=\; \inf_{|\mathbf{m}|\leq 1} \mathcal{E}_{\text{rel}}[\mathbf{m}].$$

The saturation field strength h_s is defined as the field strength at which $\mathbf{m} = \mathbf{e}_1 \chi_\Omega$ looses its energetic optimality in terms of the relaxed energy $\mathcal{E}_{\text{rel}}$ and is expected to be close to h_{c_1} when $\varepsilon \ll 1$.

To understand better the behavior of $\mathcal{E}_{\text{rel}}$, let us first introduce the notation for the average of a quantity $f = f(x_1, x_2, x_3)$ over T at fixed $x_1 \in \mathbb{R}$. We use the notation $\overline{f}(x_1) := \frac{1}{\ell^2} \int_{\text{T}} f(x_1, \cdot)$. We note that the solutions of (2.3) have the following basic properties (the proof is by an elementary integration by parts):

Lemma 2.1. *Let $\mathbf{h} \in L^2(\mathbb{R} \times \text{T}; \mathbb{R}^3)$ be a solution of (2.3). Then*

$$\overline{h}_1(x_1) = -\overline{m}_1(x_1) \qquad \text{for a.e. } x_1 \in \mathbb{R}, \tag{2.10}$$

$$\int_\Omega \mathbf{h} \cdot \mathbf{m} = -\int_{\mathbb{R}\times\text{T}} |\mathbf{h}|^2, \qquad \int_{\mathbb{R}\times\text{T}} |\mathbf{h}|^2 \;\leq \int_\Omega |\mathbf{m}|^2. \tag{2.11}$$

Using (2.10) and (2.11), one easily computes that

$$\mathcal{E}_{\rm rel}[\mathbf{m}] \overset{(2.10),(2.11)}{\geq} \int_\Omega (h_{\rm ext}+h_1)^2 \overset{(2.10)}{\geq} \int_\Omega (h_{\rm ext}-\overline{m}_1)^2, \tag{2.12}$$

where we have used Jensen's inequality in the second inequality. Hence,

$$\mathcal{E}_{\rm rel}[\mathbf{m}] \geq \inf_{|\mathbf{m}|\leq 1} \int_\Omega (h_{\rm ext}-\overline{m}_1)^2 = \begin{cases} 0, & 0 < h_{\rm ext} \leq 1, \\ \ell^2(1-h_{\rm ext})^2, & h_{\rm ext} > 1. \end{cases} \tag{2.13}$$

On the other hand, equality in (2.13) is achieved by using the trial function $\mathbf{m} = \min\{1, h_{\rm ext}\}\,\mathbf{e}_1\chi_\Omega$. Therefore, $\mathbf{m} = \mathbf{e}_1\chi_\Omega$ is the minimizer of (2.13) if and only if $h_{\rm ext} \geq h_s = 1$, which is precisely the saturation field.

Since we are interested in the bifurcation from the uniform to a patterned magnetization occurring near saturation, we introduce a parameter λ which measures the deviation from saturation:

$$h_{\rm ext} = 1 - \lambda, \tag{2.14}$$

where $0 < \lambda \ll 1$ means the applied field is just below the saturation threshold. One question we want to address is how to calculate λ_{c_0} and λ_{c_1} corresponding to the critical fields h_{c_0} and h_{c_1}.

Reformulation of the sharp interface energy: We now derive an expression for energies $\mathcal{E}$ and E in new variables which make our analysis more convenient. We introduce

$$\mathbf{u} = \mathbf{m} - (1-\lambda)\chi_\Omega \mathbf{e}_1, \qquad\qquad \mathbf{v} = \mathbf{h} + (1-\lambda)\chi_\Omega \mathbf{e}_1. \tag{2.15}$$

Then, using Lemma 2.1, (2.14), (2.11) and (2.15), one gets

$$\int_\Omega \left(h_{\rm ext}^2 - \mathbf{h}\cdot\mathbf{m} - 2\mathbf{h}_{\rm ext}\cdot\mathbf{m}\right) = \int_{\mathbb{R}\times \mathrm{T}} |\mathbf{v}|^2 - 2(1-\lambda)\int_\Omega (v_1+u_1) \overset{(2.10)}{=} \int_{\mathbb{R}\times\mathrm{T}} |\mathbf{v}|^2.$$

Therefore, we can rewrite the energy E from (2.7) as follows (with a slight abuse of notation, we view E from now on as a function of $\mathbf{u}$ instead of $\mathbf{m}$)

$$E[\mathbf{u}] = \varepsilon \int_\Omega |\nabla u_1^\delta| + Q\int_{\{|\mathbf{u}_\perp|<\delta\}} |\mathbf{u}_\perp|^2 + \int_{\mathbb{R}\times\mathrm{T}} |\mathbf{v}|^2 + \delta^2 Q \int_{\{|\mathbf{u}_\perp|\geq\delta\}} |\mathbf{u}_\perp|^2, \tag{2.16}$$

where, as before, u_1 and $\mathbf{u}_\perp$ denote the components of $\mathbf{u}$ along and normal to the easy axis, respectively, $u_1^\delta = m_1^\delta - 1 + \lambda$, and $\mathbf{v}$ solves

$$\mathbf{v} = -\nabla\varphi, \qquad \Delta\varphi = \nabla\cdot\mathbf{u} \qquad\qquad \text{in} \quad \mathbb{R}\times\mathrm{T}, \tag{2.17}$$

The set of admissible functions for (2.16) is given by

$$\mathcal{A} = \left\{\mathbf{u} \in BV(\mathbb{R}\times\mathrm{T};\mathbb{R}^3) \;:\; |\mathbf{u} + (1-\lambda)\chi_\Omega\mathbf{e}_1| = \chi_\Omega\right\}.$$

Similarly, the expression in (2.2) can be rewritten as

$$\mathcal{E}[\mathbf{u}] = \int_\Omega \frac{\varepsilon^2}{4Q}|\nabla\mathbf{u}|^2 + Q\int_\Omega |\mathbf{u}_\perp|^2 + \int_{\mathbb{R}\times\mathrm{T}} |\mathbf{v}|^2. \tag{2.18}$$

For simplicity of notation, we take the same admissible class $\mathcal{A}$ for $\mathcal{E}$ as well, setting $\mathcal{E}[\mathbf{u}] = +\infty$, whenever $\mathbf{u}_{|\Omega} \notin H^1(\Omega)$.

3 Scaling of the energy in bulk samples

In this section, we investigate the scaling behavior of the energy of minimizers in the case of bulk samples corresponding to the limit $\varepsilon \to 0$. The main part of this section will be concerned with the sharp interface energy E defined in (2.16). The connection to the diffuse interface energy $\mathcal{E}$ is then shown in Section 3.5.

The model has three dimensionless parameters: ε, λ, Q. In particular, we are interested in the case of macroscopically large samples near critical fields, i.e. $\varepsilon \ll 1$ and $\lambda \ll 1$. Our result shows that for sufficiently small ε and λ with fixed Q there are exactly two different scaling regimes, each corresponding to a particular pattern of magnetization attaining the minimal energy scale. Introducing

$$\gamma = \frac{Q}{1+Q}, \tag{3.1}$$

we have the following result for the sharp interface energy E:

Theorem 3.1. *Let $\lambda \lesssim \gamma^2 |\ln \lambda|^2$ and $\ell \gtrsim \gamma^{-\frac{1}{3}} \varepsilon^{\frac{1}{3}} \lambda^{-\frac{1}{2}} |\ln \varepsilon|^{-\frac{1}{3}}$. Then for $\varepsilon \ll 1$ and $\lambda \ll 1$, we have*

$$\frac{1}{\ell^2} \inf_{\mathbf{u} \in \mathcal{A}} E[\mathbf{u}] \;\sim\; \min\left\{ \lambda^2,\; \gamma^{\frac{1}{3}} \varepsilon^{\frac{2}{3}} \lambda |\ln \lambda|^{\frac{1}{3}} \right\}.$$

The first regime corresponds to a uniform magnetization along the applied field, while the second regime is achieved by branched magnetization patterns. Note that as long as $Q \gtrsim 1$, the particular value of Q does not affect the scaling of the minimal energy. This indicates that the restricted model corresponding to $Q = \infty$, i.e. when $\mathbf{m} = \pm \mathbf{e}_1 \chi_\Omega$, captures the essential features of the general model in (2.16). On the other hand, for $Q \ll 1$ the effect of anisotropy only has the effect of renormalizing the minimal energy scaling by a factor of $Q^{\frac{1}{3}}$. This will be further discussed in Sec. 4 with the help of a reduced sharp interface model.

Combining the results in Theorem 3.1 with (2.9) and the constructions of Sec. 3.5, the full micromagnetic energy $\mathcal{E}$ satisfies the same scaling

Theorem 3.2. *Let $\lambda \lesssim \gamma^2 |\ln \lambda|^2$ and $\ell \gtrsim \gamma^{-\frac{1}{3}} \varepsilon^{\frac{1}{3}} \lambda^{-\frac{1}{2}} |\ln \varepsilon|^{-\frac{1}{3}}$. Then for $\varepsilon \ll 1$ and $\lambda \ll 1$, we have*

$$\frac{1}{\ell^2} \inf_{\mathbf{u} \in \mathcal{A}} \mathcal{E}[\mathbf{u}] \;\sim\; \begin{cases} \lambda^2 & \text{for } \lambda \lesssim \gamma^{\frac{1}{3}} \varepsilon^{\frac{2}{3}} |\ln \varepsilon|^{\frac{1}{3}}, \\ \gamma^{\frac{1}{3}} \varepsilon^{\frac{2}{3}} \lambda |\ln \lambda|^{\frac{1}{3}} & \text{for } \lambda \gtrsim \gamma^{\frac{1}{3}} \varepsilon^{\frac{2}{3}} |\ln \varepsilon|^{\frac{1}{3}}. \end{cases}$$

This theorem implies that for small enough values of $\lambda(\varepsilon)$ the minimal energy scaling is achieved by uniform magnetization pattern (the monodomain state: $\mathbf{m} = \mathbf{e}_1 \chi_\Omega$), while for sufficiently large values of $\lambda(\varepsilon)$ the optimal energy scaling is achieved by a branched domain pattern, as $\varepsilon \to 0$. The transition occurs at $\lambda_c \sim \gamma^{\frac{1}{3}} \varepsilon^{\frac{2}{3}} |\ln \varepsilon|^{\frac{1}{3}}$.

The analysis techniques we employ in this section go back to the work of Choksi and Kohn in [6, 7], who analyzed the energy of ferromagnetic plates in the absence of a magnetic field. In our analysis we identify the optimal dependence of the minimal energy on the parameter λ which is not addressed in [6, 7]. In our analysis, we also apply tools from related works in the framework of type-I superconductors [5]. There the authors derive the scaling of the energy for the type-I superconductor near critical field. We note that the super conductor model is more rigid, since there the two different phases are described by the characteristic function χ which only takes the discrete values 0 and 1 and a divergence free magnetic field B, whereas in our model the magnetization $\mathbf{m}$ is allowed to take all values on the unit sphere.

3.1 Preliminaries

In this section we collect some useful results before addressing the proof of the upper and lower bound in the next two sections.

Control on (2.16) yields information about u_1 and v_1 on each slice. As expected, the stray field favors zero average of u_1 on each tangential slice:

Lemma 3.3. *Let $\mathbf{u} \in \mathcal{A}$ and let $\mathbf{v} \in L^2(\mathbb{R} \times \mathrm{T}; \mathbb{R}^3)$ satisfy (2.17). Then for every $c_1 > 0$ and $c_2 > 0$ there exists a constant $c > 0$, such that if $E[\mathbf{u}]/\ell^2 \leq c\lambda^2$ then we have*

$$\int_0^1 |\overline{u}_1|^2 dx_1 \;\leq\; c_1^2 \lambda^2. \tag{3.2}$$

Furthermore there exists $I \subseteq (0,1)$ with $|I| > 1 - c_2$, such that for all $a \in I$

$$|\overline{u}_1(a)| \;\leq\; c_1 \lambda. \tag{3.3}$$

Proof. We first note that in terms of $\mathbf{u}$ and $\mathbf{v}$, in view of (2.10), we have $\bar{v}_1 = -\bar{u}_1$ for a.e. $a \in \mathbb{R}$. By Jensen's inequality, it then follows that

$$\ell^2 \int_0^1 |\overline{u}_1|^2 dx_1 \;=\; \int_\Omega |\overline{u}_1|^2 \;=\; \int_\Omega |\overline{\mathbf{v}}|^2 \;\leq\; \int_\Omega |\mathbf{v}|^2 \;\leq\; E[\mathbf{u}],$$

and (3.2) follows. Inequality (3.3) follows from (3.2) by an application of Fubini's Theorem. □

The main ingredient for the proof of the lower bound is an estimate that characterizes the transition energy, i.e. the cost for the magnetization to vary between a tangential slice $\{a\} \times \mathrm{T}$ and its value zero outside of the sample. The idea to estimate such transition energies was introduced in [20] and has been subsequently applied also in e.g. [5, 8].

Lemma 3.4 (Transition energy)**.** *For every $\mathbf{u} \in \mathcal{A}$ there exists $I \subset (0,1)$ with $|I| > \frac{1}{2}$, such that for all $a \in I$ and for all $\psi \in H^1(\mathrm{T})$, we have*

$$\left| \int_{\{a\} \times \mathrm{T}} u_1 \psi \right| \;\lesssim\; E^{\frac{1}{2}}[\mathbf{u}] \left(\gamma^{-\frac{1}{2}} \|\nabla \psi\|_{L^2(\mathrm{T})} + \|\psi\|_{L^2(\mathrm{T})} \right).$$

Proof. Let us first assume that $\mathbf{u} \in C_c^\infty(\mathbb{R} \times \mathrm{T})$, with $\mathbf{u} = 0$ outside of $[-1, 2] \times \mathrm{T}$. Let $\mathbf{v}$ be defined by (2.3). Noting that ψ does not depend on x_1 and using integration by parts, for any $a \in (0,1)$ and $b \in (-2, -1)$, we then get

$$\begin{aligned}
\int_{\mathrm{T}} u_1(a, \cdot) \psi \;&=\; \int_b^a \int_{\mathrm{T}} \partial_1 \big(u_1(x_1, \cdot)\, \psi \big)\, dx_1 \\
&\overset{(2.3)}{=} -\int_b^a \int_{\mathrm{T}} \nabla_\perp \cdot \mathbf{u}_\perp(x_1, \cdot)\; \psi \, dx_1 - \int_b^a \int_{\mathrm{T}} \nabla_\perp \cdot \mathbf{v}_\perp(x_1, \cdot)\; \psi \, dx_1 - \int_b^a \int_{\mathrm{T}} \partial_1 v_1(x_1, \cdot)\; \psi \, dx_1 \\
&=\; \int_b^a \int_{\mathrm{T}} \mathbf{u}_\perp(x_1, \cdot) \cdot \nabla_\perp \psi \, dx_1 + \int_b^a \int_{\mathrm{T}} \mathbf{v}_\perp(x_1, \cdot) \cdot \nabla_\perp \psi \, dx_1 + \int_{\mathrm{T}} v_1(a, \cdot) \psi \, dx_1 - \int_{\mathrm{T}} v_1(b, \cdot) \psi.
\end{aligned} \tag{3.4}$$

By Fubini's theorem, there exists $b \in (-2,-1)$ and $I \subseteq (0,1)$ with $|I| > \frac{1}{2}$ such that for all $a \in I$,

$$\int_{\{a\}\times \mathrm{T}} |v_1|^2 + \int_{\{b\}\times \mathrm{T}} |v_1|^2 \lesssim \int_{\mathbb{R}\times \mathrm{T}} |v_1|^2. \tag{3.5}$$

The statement then follows for all $a \in I$ from (3.4), (3.5) and by application of Cauchy-Schwarz inequality and (2.16).

Now consider a general $\mathbf{u} \in \mathcal{A}$. In this case, $\mathbf{u}$ can be approximated by a sequence of functions $\mathbf{u}^j \in C_c^\infty(\mathbb{R}\times \mathrm{T})$ such that $\mathbf{u}^j = 0$ outside of $[-1,2]\times \mathrm{T}$ and such that $\mathbf{u}^j \to \mathbf{u}$ in $L^2(\mathbb{R}\times \mathrm{T};\mathbb{R}^3)$ and $\int_{\mathbb{R}\times \mathrm{T}} |\nabla \mathbf{u}^j| \to \int_{\mathbb{R}\times \mathrm{T}} |\nabla \mathbf{u}|$, see [14]. By (2.11), we also have $\mathbf{v}^j \to \mathbf{v}$ in $L^2(\mathbb{R}\times \mathrm{T};\mathbb{R}^3)$, where $\mathbf{v}^j$ denotes the stray field of $\mathbf{u}^j$. Taking a subsequence, if necessary, we also have convergence $\mathbf{u}^j \to \mathbf{u}$, $\mathbf{v}^j \to \mathbf{v}$ in $L^2(\{a\}\times \mathrm{T};\mathbb{R}^3)$ for a. e. $a \in \mathbb{R}$. Using this approximation, the lemma follows. □

We will also use the following technical lemma of De Giorgi (see, e.g., [5, Lemma 3.1]):

Lemma 3.5. *Let $S \subset \mathrm{T}$ be a set of finite perimeter, and let $r > 0$ be such that $r|\partial S| \le \frac{1}{4}|S|$. Then there exists an open set $\overline{S} \subset \mathrm{T}$ with the properties*

(i) There is a considerable overlap of $\bar{S}$ with S, in the sense of $|S \cap \overline{S}| \ge \frac{1}{2}|S|$.

(ii) For all $t > 0$, the set $\overline{S}^t := \{p \in \mathrm{T} : \mathrm{dist}\,(p,\overline{S}) < t\}$ satisfies $|\overline{S}^t| \lesssim |S|(1+(t/r)^2)$.

3.2 Ansatz-free lower bound

In this section, we present the proof for the lower bound. We need to show:

Proposition 3.6 (Lower bound)**.** *For $\varepsilon \ll 1$ and $\lambda \ll \gamma$, we have*

$$\frac{1}{\ell^2} \inf_{\mathbf{u}\in\mathcal{A}} E[\mathbf{u}] \gtrsim \min\left\{\lambda^2,\ \gamma^{\frac{1}{3}}\varepsilon^{\frac{2}{3}}\lambda|\ln\lambda|^{\frac{1}{3}}\right\}.$$

Proof. Following the ideas in [5], we argue as follows. Recall that in view of Lemma 3.4, the energy is bounded below by a Sobolev-type norm of negative order on $\mathbf{u}$, evaluated on a generic tangential slice $\{a\}\times T$. In this proof, we combine this with control that we have on the surface energy and anisotropy energy on a generic slice. The proof is divided into five steps.

Step 1: Identification of tangential slice. We will argue by contradiction. Hence, we may assume that the energy does *not* satisfy the lower bound, i.e., there exists $\mathbf{u} \in \mathcal{A}$, such that

$$E[\mathbf{u}] \ll \ell^2 \min\left\{\lambda^2,\ \gamma^{\frac{1}{3}}\varepsilon^{\frac{2}{3}}\lambda|\ln\lambda|^{\frac{1}{3}}\right\}, \tag{3.6}$$

for some $\varepsilon \ll 1$ and $\lambda \ll \gamma$. We choose $a \in (0,1)$ such that the assertions of Lemma 3.3 and Lemma 3.4 hold. By Lemma 3.3 and by Fubini's Theorem, we may then assume that a is furthermore chosen such that

$$|\overline{u}_1(a)| \ll \lambda \tag{3.7}$$

$$\int_{\{a\}\times \mathrm{T}} |\nabla u_1| \lesssim \frac{E}{\varepsilon} \overset{(3.6)}{\ll} \ell^2 \min\left\{\frac{\lambda^2}{\varepsilon},\ \frac{\gamma^{\frac{1}{3}}\lambda|\ln\lambda|^{\frac{1}{3}}}{\varepsilon^{\frac{1}{3}}}\right\}, \tag{3.8}$$

$$\int_{\{a\}\times \mathrm{T}} |\mathbf{u}_\perp|^2 \lesssim \frac{E}{Q} \overset{(3.6)}{\ll} \ell^2 \min\left\{\frac{\lambda^2}{Q},\ \frac{\gamma^{\frac{1}{3}}\varepsilon^{\frac{2}{3}}\lambda|\ln\lambda|^{\frac{1}{3}}}{Q}\right\}. \tag{3.9}$$

Step 2: Structure of magnetization. We next analyze the magnetization on the slice $A := \{a\} \times \mathrm{T}$ in more detail. In view of the upper constructions, we expect that the regions where the magnetization points in the negative x_1-direction are small needle-shaped domains. The restriction of m_1 to the slice, therefore, is expected to be negative on a number of small circular domains. In the following, we give a precise version of this heuristic picture. We define the set A_+ (where $\mathbf{m}$ points "to the right", i.e. in direction of $\mathbf{e}_1$. The notation "to the right" is in accordance with the figures) and the set A_- (where $\mathbf{m}$ points to the left) by

$$A_+ \;:=\; \big\{x \in A \;:\; \frac{1}{2}\lambda < u_1 \le \lambda\big\}, \qquad\qquad A_- \;:=\; \big\{x \in A \;:\; -2+\lambda \le u_1 < -1+\lambda\big\}.$$

It is also convenient to define a transition region A_0 (where $\mathbf{m}$ also points to the right)

$$A_0 := \big\{x \in A \;:\; -1+\lambda \le u_1 \le \frac{1}{2}\lambda\big\}.$$

We first note that when $m_1 \ge 0$, we have $|\mathbf{u}_\perp|^2 = |\mathbf{m}_\perp|^2 = 1 - m_1^2 \ge 1 - m_1 = \lambda - u_1$, i.e.

$$|\mathbf{u}_\perp|^2 \;\ge\; \lambda - u_1 \qquad\qquad \text{in } A_0 \cup A_+. \tag{3.10}$$

We claim that the region A_- of "reversed magnetization" is concentrated on a small set with total area of order $\lambda\ell^2$, and that the transition region is even smaller. More precisely, we claim that

$$|A_+| \;\sim\; \ell^2, \qquad\qquad |A_0| \;\ll\; \lambda\ell^2, \qquad\qquad |A_-| \;\sim\; \lambda\ell^2. \tag{3.11}$$

Indeed, by (3.10), we have $|\mathbf{u}_\perp|^2 \ge \frac{\lambda}{2}$ in A_0, and so

$$|A_0| \;\le\; \frac{2}{\lambda}\int_{A_0} |\mathbf{u}_\perp|^2 \;\lesssim\; \frac{E}{\lambda Q} \overset{(3.9)}{\ll} \ell^2.$$

Here we also have used that by assumption $Q \ge \gamma \gg \lambda$. Choosing $c_1 = \frac{1}{16}$ in Lemma 3.3, and in view of $|A_0| + |A_+| = \ell^2 - |A_-|$, we get

$$-\tfrac{1}{16}\lambda\ell^2 \overset{(3.3)}{\le} \int_A u_1 \;\le\; (-1+\lambda)|A_-| + \lambda(|A_0| + |A_+|) \;=\; -|A_-| + \lambda\ell^2,$$

so $|A_-| \le \frac{17}{16}\lambda\ell^2 \ll \ell^2$ and, therefore, $|A_+| \ge \frac{1}{2}\ell^2$. Similarly,

$$\begin{aligned} -\tfrac{1}{16}\lambda\ell^2 &\overset{(3.3)}{\le} -\int_A u_1 \;\le\; 2|A_-| + \int_{A_0} (\lambda - u_1) - \tfrac{1}{2}\lambda|A_+| \\ &\overset{(3.10)}{\le} 2|A_-| + \int_{A_0} |\mathbf{u}_\perp|^2 - \tfrac{1}{4}\lambda\ell^2 \le\; 2|A_-| + \frac{CE}{Q} - \tfrac{1}{4}\lambda\ell^2 \overset{(3.9)}{\le} 2|A_-| - \tfrac{1}{8}\lambda\ell^2. \end{aligned}$$

Hence $|A_-| \ge \frac{1}{32}\lambda\ell^2$, and so $|A_-| \sim \lambda\ell^2$. This concludes the proof of (3.11).

Step 3: Identification of a regularized region. In the previous step, we showed that the reversed magnetization region A_- occupies a small fraction of A. By the upper bound constructions of Lemma 3.8 below, we would expect that A_- is divided into a controlled number of similar size

circular domains. The construction also suggests that in the core region of the plate, the typical radius r of these circular domains and the typical distance a between them are given by

$$r \;=\; \frac{\varepsilon^{\frac{1}{3}}}{\gamma^{\frac{1}{3}}|\ln\lambda|^{\frac{1}{3}}}, \qquad\qquad a \;=\; \frac{\varepsilon^{\frac{1}{3}}}{\gamma^{\frac{1}{3}}\lambda^{\frac{1}{2}}|\ln\lambda|^{\frac{1}{3}}}. \tag{3.12}$$

In the following, we use the co-area formula and the isoperimetric inequality to get a rigorous variant of the above heuristics. We replace A_- by a larger set S with $A_- \subseteq S \subseteq A_- \cup A_0$. The reason to choose S instead of A_- is that we cannot exclude a concentration of surface energy on ∂A_-. We claim that there is $c \in (-\frac{1}{2}, -\frac{1}{4})$ such that the set

$$S \;:=\; \left\{\; x \in A \;:\; u_1 < c \;\right\} \tag{3.13}$$

satisfies

$$|S| \;\sim\; \lambda\ell^2, \tag{3.14}$$

$$|\partial S| \overset{(3.8)}{\ll} \ell^2 \min\left\{\frac{\lambda^2}{\varepsilon},\; \frac{\gamma^{\frac{1}{3}}\lambda|\ln\lambda|^{\frac{1}{3}}}{\varepsilon^{\frac{1}{3}}}\right\}. \tag{3.15}$$

Indeed, by (3.13) it follows that $A_- \subseteq S \subseteq A_- \cup A_0$ and (3.14) follows by (3.11). Furthermore, by the co-area formula

$$\int_A |\nabla_\perp u_1| \;=\; \int_{\mathbb{R}} \mathcal{H}^1(\{x_\perp \in A : u_1(x_\perp) = t\})\; dt,$$

and Fubini's Theorem, there exists $c \in (-\frac{1}{2}, -\frac{1}{4})$, such that S satisfies

$$|\partial S| \;\lesssim\; \int_A |\nabla_\perp u_1| \overset{(3.8)}{\ll} \ell^2 \min\left\{\frac{\lambda^2}{\varepsilon},\; \frac{\gamma^{\frac{1}{3}}\lambda|\ln\lambda|^{\frac{1}{3}}}{\varepsilon^{\frac{1}{3}}}\right\}.$$

Estimates (3.14) and (3.15) together with (3.12) yield

$$r\;|\partial S| \;\ll\; |S|. \tag{3.16}$$

Heuristically, the estimate in (3.16) means that S, roughly speaking, splits into a collection of disks of diameter much larger than r. This disagrees with the expectation from the upper construction and will lead to a contradiction.

We next replace S by another set $\overline{S}$, still satisfying all the relevant properties of S. Additionally, it grows in a controlled way upon "thickening". More precisely, in view of (3.16) and by Lemma 3.5, there is a set $\overline{S}$ with

$$|S \cap \overline{S}| \;\geq\; \frac{1}{2}|S| \overset{(3.14)}{\gtrsim} \lambda\ell^2 \tag{3.17}$$

and such that for all $t \geq r$, the t-neighborhood $\overline{S}^t$ of $\overline{S}$ satisfies

$$|\overline{S}^t| \;\lesssim\; \frac{t^2}{r^2}|S| \overset{(3.14)}{\lesssim} \frac{\lambda t^2 \ell^2}{r^2}. \tag{3.18}$$

Step 4: Definition of a suitable test function. We now define a logarithmic cut-off $\psi \in H^1(\mathrm{T})$, with $0 \le \psi \le 1$, around $\overline{S}$. Let

$$\psi(x_\perp) \;:=\; \varphi(\mathrm{dist}\,(x_\perp, \overline{S})), \qquad \text{where} \qquad \varphi(t) \;:=\; \begin{cases} 1 & \text{for } 0 \le t \le r, \\ \frac{\ln(a/t)}{\ln(a/r)} & \text{for } r \le t \le a, \\ 0 & \text{for } a \le t, \end{cases} \tag{3.19}$$

with r and a defined in (3.12). A direct computation, following [5], then yields

$$\int_{\mathrm{T}} \psi \;\lesssim\; \frac{\ell^2}{|\ln \lambda|} \qquad \text{and} \qquad \int_{\mathrm{T}} |\nabla \psi|^2 \;\lesssim\; \frac{\ell^2}{a^2 |\ln \lambda|}. \tag{3.20}$$

For the reader's convenience, we show the first estimate in (3.20), the proof of the second inequality proceeds similarly. Since $\psi = 1$ on $\overline{S}$, and since $|\partial \overline{S}^t| = \frac{d}{dt} |\overline{S}^t|$, we have

$$\begin{aligned} \int_T \psi \;&=\; |\overline{S}| + \int_0^\infty \varphi(t)\; |\partial \bar{S}^t|\; dt = \; -\int_r^a \varphi'(t)\; |\bar{S}^t|\; dt \\ &\overset{(3.18)}{\lesssim} \frac{\lambda \ell^2}{r^2 |\ln a/r|} \int_0^a t\; dt \;\lesssim\; \frac{\lambda a^2 \ell^2}{r^2 |\ln \lambda|} \overset{(3.12)}{=} \frac{\ell^2}{|\ln \lambda|}. \end{aligned}$$

Step 5: Proof of the lower bound. We are ready to give the proof of the lower bound. It is based on application of Lemma 3.4 and on a duality argument, using the test function ψ. We claim that

$$\lambda \ell^2 \;\lesssim\; -\int_A u_1 \psi. \tag{3.21}$$

Since $\psi = 1$ and $u_1 \le -\frac{1}{4}$ in S, and since $\psi \ge 0$ and $u_1 \le \lambda$ in A, it follows for $\lambda \ll 1$ that

$$-\int_A u_1 \psi \;=\; -\int_{S \cap \overline{S}} u_1 \psi - \int_{A \setminus (S \cap \overline{S})} u_1 \psi \;\ge\; \frac{1}{4} |S \cap \overline{S}| - \lambda \int_A \psi \overset{(3.14),(3.17)}{\gtrsim} \lambda \ell^2.$$

Application of Lemma 3.4 then yields

$$\lambda \ell^2 \overset{(3.21)}{\lesssim} -\int_A u_1 \psi \;\lesssim\; E^{\frac{1}{2}}[\mathbf{u}] \left(\frac{1}{\gamma^{\frac{1}{2}}} \|\nabla \psi\|_{L^2(\mathrm{T})} + \|\psi\|_{L^2(\mathrm{T})} \right) \overset{(3.20)}{\lesssim} E^{\frac{1}{2}}[\mathbf{u}] \left(\frac{\ell^2}{\gamma a^2 |\ln \lambda|} + \ell^2 \right)^{\frac{1}{2}}.$$

We hence obtain

$$E[\mathbf{u}] \;\gtrsim\; \ell^2 \min\left\{ \gamma \lambda^2 a^2 |\ln \lambda|, \lambda^2 \right\} \overset{(3.12)}{=} \ell^2 \min\left\{ \gamma^{\frac{1}{3}} \varepsilon^{\frac{2}{3}} \lambda^{\frac{1}{3}} |\ln \lambda|,\; \lambda^2 \right\},$$

contradicting (3.6). This concludes the proof of the Proposition. □

3.3 Sharp interface constructions

In this section, we present constructions that achieve the optimal scaling in Theorem 3.1. We have two different regimes. For smaller values of λ, the optimal scaling of the energy is achieved by a uniform configuration, while for larger values of λ, the optimal scaling is achieved by a self–similar structure. Note that the constructions in [6] do not yield the optimal energy in the case of near

saturation field. Instead, our constructions are an adaptation of constructions introduced in [5] for a model of type-I superconductors. While our constructions have a similar self–repeating structure to that of [6], the definition of the involved functions is different due to the constraint $|\mathbf{m}| = \chi_\Omega$ in our model. Our constructions are also different from those of [5] in the geometry of the magnetic domains, and are intended to better mimic the behavior of the minimizers. The main result of this section is:

Proposition 3.7 (Upper bound)**.** *Suppose that $\lambda \lesssim \gamma^2 |\ln \lambda|^2$. Then for $\varepsilon \ll 1$ and $\lambda \ll 1$, the scaling of the minimal energy E is bounded above by*

$$\frac{1}{\ell^2} \inf_{\mathbf{u}\in\mathcal{A}} E[\mathbf{u}] \;\lesssim\; \min\left\{\lambda^2,\; \gamma^{\frac{1}{3}}\varepsilon^{\frac{2}{3}}\lambda|\ln\lambda|^{\frac{1}{3}}\right\}.$$

Let us remark that the logarithm in the scaling of the energy is a consequence of the fact that the leading order contribution of the stray field energy is given by interaction on tangential slices, where the stray field potential behaves logarithmically.

We first note that by choosing the uniform magnetization $\mathbf{u} = \lambda \mathbf{e}_1 \chi_\Omega$, we immediately recover the upper bound $\frac{1}{\ell^2}\inf_{\mathbf{u}\in\mathcal{A}} E[\mathbf{u}] \;\lesssim\; \lambda^2$. The cross–over to the branched regime occurs at $\lambda \sim \gamma^{\frac{1}{3}}\varepsilon^{\frac{2}{3}}|\ln\lambda|^{\frac{1}{3}}$. It hence remains to construct an optimal upper bound, if λ is larger than this threshold. In the remaining part of this section, we present such a construction. The corresponding estimates are then given in Section 3.4, thus completing the proof of Proposition 3.7.

Before going into the details of our constructions, however, let us recall some other constructions that have been proposed in the literature over the years (for simplicity, we will only discuss the case $Q \sim 1$). The first estimates of the minimal energy for the bulk uniaxial ferromagnets go back to the work of Landau and Lifshitz [24] and Kittel [18]. Those constructions were proposed for zero applied field. In fact, the Landau-Lifshitz construction cannot be easily extended to the case when the domains opposing the applied field occupy only a small volume fraction of the sample. The Kittel construction, on the other hand, can be modified to account for small volume fraction, resulting in an energy scaling $E\ell^{-2} \sim \varepsilon^{\frac{1}{2}}\lambda|\ln\lambda|$ [22]. However, since it consists of a "striped" domain pattern, its interfacial energy turns out to be too high at small λ. This issue can be addressed by modifying the geometry of the domains into a lattice of cylindrical "bubbles", whose energy my be estimated as $E\ell^{-2} \sim \varepsilon^{\frac{1}{2}}\lambda$ [3, 13]. A comparison of this estimate with the result of Proposition 3.6 shows that, although the bubble construction provides a slight improvement over the stripe construction, it is highly non-optimal in its scaling behavior with respect to ε. We note that, in fact, any domain configuration, in which the domain walls are aligned with the easy axis cannot do better in terms of energy, and so branching is inevitable for sufficiently small ε to reduce energy [7]. On the other hand, if a tree-like branched domain structure is used (see [8, Sec. 4.3] for the construction in the case of type-I superconductors), it is not difficult to show that the energy will scale as $E\ell^{-2} \sim \varepsilon^{\frac{2}{3}}\lambda^{\frac{2}{3}}$. Once again, comparing this with the result of Proposition 3.6, one sees that, while the considered configuration gives the optimal scaling in terms of the dependence of the energy on ε, it is highly non-optimal in terms of λ. These observations indicate that the minimizers of E may not have the geometric characteristics of any of the domain patterns considered above when $\varepsilon \ll 1$ and $\lambda \ll 1$. In the following we present a construction which achieves the scaling in Proposition 3.6, thus demonstrating that this scaling is optimal.

We begin by fixing the basic geometry. The geometry is an adaption of a recent self-similar construction for the type-I superconductor model [5]. However, contrary to the construction in [5],

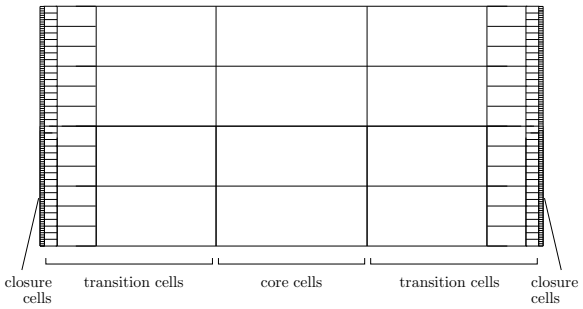

Figure 3: A side view (in the x_1x_2-plane) of a sample partition containing 16 core cells with 4 generations of refining cells on each side.

our construction includes closure domains. These closure domains are, in particular, necessary to achieve the optimal scaling of the energy in the case of soft materials, i.e. $Q \ll 1$. Based on this geometry, we construct two different magnetization configurations $\mathbf{u}^{AF}$ and $\mathbf{u}^{SF}$. The first configuration $\mathbf{u}^{AF}$ avoids anisotropy energy entirely and is optimal for $Q \gtrsim 1$. The second configuration $\mathbf{u}^{SF}$ avoids most of the stray fields and is optimal for $Q \lesssim 1$.

Sample geometry. We divide the material plate into three spatial regions: the core region, the transition region and the surface region, see Fig. 3. These regions form 5 layers symmetrically with respect to the plate's mid-plane. By this symmetry, it is, therefore, sufficient to describe the constructions only in the left half of the sample, i.e. for $0 \le x_1 \le \frac{1}{2}$.

The core region is partitioned into equal rectangular cells with height h_0 in the normal direction (x_1-direction) and length a_0 in both tangential directions. These cells are adjacent on the left to a system of M layers of self-similar cells in the transition and surface regions that refine from the core region towards the boundary (see Fig. 3). Each generation of cells is described by its height h_j in the normal direction and its extension a_j in both tangential directions, with $j = 1, \dots, M$. We also define a parameter $r_j = \lambda^{\frac{1}{2}} a_j / \sqrt{2\pi}$, which will be the maximum needle radius in the j-th generation of cells. In every generation, the width of the cells decreases by a factor 3, i.e.

$$a_{j+1} \;=\; \frac{a_j}{3} \qquad \text{and} \qquad r_{j+1} \;=\; \frac{r_j}{3}. \tag{3.22}$$

In particular, the number of cells is multiplied by a factor 9 in each new generation. The algorithm is terminated after M iterations. We will specify a_1, $\{h_j\}$, and M in the sequel. In particular, these parameters will be chosen, such that the union of all cells exactly covers Ω, i.e.

$$h_0 + 2\sum_{j=1}^{M} h_j \;=\; 1. \tag{3.23}$$

We differentiate between core cells (which for simplicity of notation we identify with generation 0), transition cells (generations 1, ..., $M-1$) and closure cells (generation M).

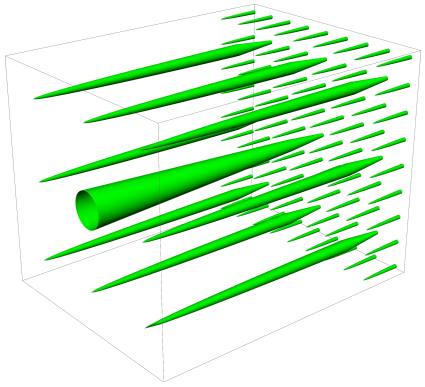

Figure 4: Refinement towards the sample boundary (two generations are shown).

Globally, the geometry of the construction consists of a collection of needles rescaled to fit into the collection of cells just constructed, refining in the direction of the boundary, see Fig. 4. We capture the region occupied by the needles by the characteristic function $\chi \in BV(\mathbb{R}^3, \{0,1\})$, which will be specified in the sequel. We thus give the definition of χ on a rescaled cell

$$Z \;=\; [0,h] \times K, \qquad\qquad K = \left[-\tfrac{a}{2}, \tfrac{a}{2}\right]^2, \tag{3.24}$$

with height h and width a. We furthermore denote the tangential boundary of the cell by $\partial_\perp Z := [0,h] \times \partial K$. The corresponding "maximum needle radius" r is defined by

$$r = \left(\frac{\lambda}{2\pi}\right)^{\frac{1}{2}} a. \tag{3.25}$$

The definition of χ on any cell with arbitrary extension (in the left side of the sample) is then given by a rescaling of this cell.

Geometry of a transition cell. Consider a transition cell Z_{trns} first. The cell geometry is characterized by nine needles, see Fig. 5(a). The largest needle is located in the center of the cell and grows into positive x_1–direction, while the other needles are smaller and grow in the negative x_1-direction. All needles are axially-symmetric around their corresponding center lines given by $x_\perp = x_\perp^{(i)}$, $i = 1, \ldots, 9$. The large needle is located in the center of the cell, i.e. $x_\perp^{(1)} = 0$. The radii of the needle cross-sections on tangential slices are functions of x_1. The radius of the large needle is denoted by $\rho_1(x_1) := \rho_+(x_1)$. The radii of the 8 small needles are given by $\rho_i(x_1) := \rho_-(x_1)$ for $i = 2, \ldots 9$. The characteristic function χ is defined by

$$\chi(x_1, x_\perp) \;:=\; \sum_{i=1}^{9} H(\rho_i(x_1) - |x_\perp - x_\perp^{(i)}|) \qquad\qquad \text{for } (x_1, x_\perp) \in Z_{\text{trns}}, \tag{3.26}$$

where H is the Heaviside function, i.e., $H(s) = 1$ for $s > 0$ and $H(s) = 0$ for $s \leq 0$. It remains to specify the radii $\rho_\pm$ for the large and small needles.

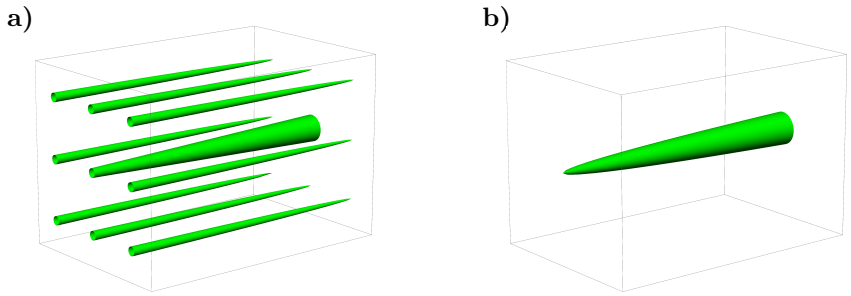

Figure 5: Geometry of a unit cell: a) transition cell; b) closure cell.

At the tangential faces, i.e. at $x_1 = 0$ and $x_1 = h$, of the cell the needle radii are defined by

$$\rho_+(0) = \rho_-(0) = \tfrac{1}{3}r, \qquad\qquad \rho_-(h) = 0, \quad \rho_+(h) = r,$$

respectively. This means that at $x_1 = 0$ all needles have the same radius. At $x_1 = h$, the radii of the small needles are zero. We choose $\rho_\pm$, such that throughout the cell, the cross-sectional area of the needles is constant, i.e.

$$\pi\rho_+^2(x_1) + 8\pi\rho_-^2(x_1) \;=\; \tfrac{1}{2}\lambda a^2. \tag{3.27}$$

To avoid further complicating the constructions, we assume that the profile of the small needles is conical at the tip:

$$h\rho_-(x_1) \;=\; r(h - x_1), \qquad\qquad \text{for } (1-\alpha)h \le x_1 \le h, \tag{3.28}$$

where $0 < \alpha \ll 1$. The precise value of α is inconsequential and, in fact, for the zero anisotropy configuration $\mathbf{u}^{AF}$ could even be taken to be zero. In view of (3.27), equation (3.28) defines $\rho_+(x_1)$ for $(1-\alpha)h \le x_1 \le h$. Furthermore, on most of the cell, i.e. for $0 \le x_1 \le (1-\alpha)h$, we choose ρ_+ to be the linear interpolation connecting the values of ρ_+ at $x_1 = 0$ and $x_1 = (1-\alpha)h$. In turn, ρ_- is defined by (3.27). Note that as a consequence of the conical profile at the tip of the small needles (see (3.28)), it follows that

$$|\rho_+'(x_1)|,\ |\rho_-'(x_1)| \;\lesssim\; \frac{r}{h} \qquad\qquad \text{for all } x_1 \in [0,h]. \tag{3.29}$$

Geometry of a closure cell. In any closure domain cell $Z_{\rm cls}$, there is only one large needle along the center of the cell, see 5(b). The radius $\rho_{\rm cls}(x_1)$ satisfies the conditions $\rho_{\rm cls}(0) = 0$ and $\rho_{\rm cls}(h) = r$. Analogously to the above construction for the transition cell, we choose a needle shape with a conical tip. Define

$$\chi(x_1, x_\perp) \;:=\; H(\rho_{\rm cls}(x_1) - |x_\perp|) \qquad\qquad \text{for } x \in Z_{\rm cls}. \tag{3.30}$$

In particular, we also have

$$|\rho_{\rm cls}'(x_1)| \;\lesssim\; \frac{r}{h} \qquad\qquad \text{for all } x_1 \in [0,h]. \tag{3.31}$$

Geometry of a core cell. In each core cell $Z_{\rm core}$ the function χ is assumed to be a characteristic function of a straight cylinder with the radius equal to that of the needle on the adjacent side of the transition cell. The overall geometry of the magnetization pattern for one core cell and 3 refining generations is presented in Fig. 1. In the sequel, we give two different magnetization configurations, $\mathbf{u}^{AF}$ and $\mathbf{u}^{SF}$, based on the geometry described above.

The magnetization $\mathbf{u}^{AF}$. We first define the anisotropy-free configuration $\mathbf{u}^{AF}$ by

$$\mathbf{u}^{AF}(x) \;:=\; \big(\lambda - 2\chi(x)\big)\mathbf{e}_1 \qquad\qquad \text{in } Z_{\rm core}, Z_{\rm trns}, Z_{\rm cls}, \tag{3.32}$$

and zero outside Ω. Note that the stray field of $\mathbf{u}^{AF}$ is created by surface charges on the needle interfaces and at the sample surface. We next define an auxiliary field $\tilde{\mathbf{v}}^{AF}$. In every transition cell $Z_{\rm trns}$, we define

$$\tilde{\mathbf{v}}^{AF} := \; -\nabla_\perp \varphi \qquad\qquad \text{in } Z_{\rm trns}, \tag{3.33}$$

where φ is a solution of

$$\Delta_\perp \varphi \;=\; \nabla\cdot \mathbf{u}^{AF} \quad \text{in } Z_{\rm trns} \qquad\qquad \text{and} \qquad\qquad \partial_{\boldsymbol{\nu}_\perp}\varphi \;=\; 0 \quad \text{on } \partial_\perp Z_{\rm trns}. \tag{3.34}$$

Note that $\mathbf{v}^{AF}$ is uniquely defined, since by (3.26) and (3.27) we have

$$\int_K u_1^{AF}(x_1, x_\perp)\, dx_\perp = 0 \qquad\qquad \forall x_1 \in [0,h], \tag{3.35}$$

implying the solvability condition for (3.34), in view of the fact that $\mathbf{u}^{AF} = u_1^{AF}\mathbf{e}_1$. Also note that the corresponding field $\tilde{\mathbf{v}}^{AF}$ is the approximation of the stray field assuming that magnetostatic interactions in tangential slices are dominant.

In closure domain cells, (3.35) does not hold any more. Hence, in this case we define $\tilde{\mathbf{v}}^{AF}$ by

$$\tilde{\mathbf{v}}^{AF} \;=\; -\nabla_\perp \varphi_1 - \partial_1 \varphi_2 \; \mathbf{e}_1 \qquad\qquad \text{in } Z_{\rm cls}, \tag{3.36}$$

where $\nabla_\perp \varphi_1$ approximates stray field interaction in tangential directions, while $\partial_1\varphi_2$ approximates stray field interaction in the normal direction. We define φ_1 as a solution of

$$\Delta_\perp \varphi_1 \;=\; \nabla\cdot \mathbf{u}^{AF} - \tfrac{1}{a^2}\textstyle\int_K \nabla\cdot \mathbf{u}^{AF}(x_1, \hat{x}_\perp)\, d\hat{x}_\perp \quad \text{in } Z_{\rm cls} \quad \text{and} \quad \partial_{\nu_\perp}\varphi_1 \;=\; 0 \quad \text{on } \partial_\perp Z_{\rm cls}. \tag{3.37}$$

The function φ_2 is defined as a solution of

$$\partial_1^2 \varphi_2(x_1) = \tfrac{1}{a^2}\textstyle\int_K \nabla\cdot \mathbf{u}^{AF}(x_1, \hat{x}_\perp)\, d\hat{x}_\perp \quad \text{in } Z_{\rm cls} \qquad \text{and} \qquad \partial_1\varphi_2 = 0 \quad \text{on } \{x_1 = 0\}\times K. \tag{3.38}$$

Similarly to (3.34), up to a constant, problems (3.37) and (3.38) are indeed uniquely solvable for φ_1 and φ_2. Finally, we set $\tilde{\mathbf{v}}^{AF} = 0$ in the core cells $Z_{\rm core}$ and outside Ω.

The magnetization $\mathbf{u}^{SF}$. Here we construct an approximately stray field-free magnetization $\mathbf{u}^{SF}$. Although it would be natural to consider $\mathbf{u} = \mathbf{u}^{AF} + \tilde{\mathbf{v}}^{AF}$ as a trial function, in view of the fact that $\nabla\cdot\mathbf{u} = 0$ in this case, this function is not admissible, i.e. it does not belong to $\mathcal{A}$. For this reason, using the construction of $\mathbf{u}^{AF}$ and $\tilde{\mathbf{v}}^{AF}$ above, we define an auxiliary function $\tilde{\mathbf{v}}^{SF}$:

$$\tilde{\mathbf{v}}^{SF}(x) := \; \Big(1 - \sqrt{1 - |\tilde{\mathbf{v}}^{AF}(x)|^2}\;\Big)(\mathbf{u}^{AF}(x) + (1-\lambda)\chi_\Omega(x)\mathbf{e}_1) \qquad \text{in } Z_{\rm trns}, \tag{3.39}$$

$$\tilde{\mathbf{v}}^{SF}(x) := \; \Big(1 - \sqrt{1 - |\tilde{\mathbf{v}}_\perp^{AF}(x)|^2}\;\Big)(\mathbf{u}^{AF}(x) + (1-\lambda)\chi_\Omega(x)\mathbf{e}_1) + \tilde{v}_1^{AF}(x)\mathbf{e}_1 \qquad \text{in } Z_{\rm cls}. \tag{3.40}$$

As will be shown in Sec. 3.4, this definition is well-posed, since in our construction $|\tilde{\mathbf{v}}^{AF}| \ll 1$. We, therefore, set

$$\mathbf{u}^{SF} \;:=\; \mathbf{u}^{AF} + \tilde{\mathbf{v}}^{AF} - \tilde{\mathbf{v}}^{SF}. \tag{3.41}$$

It can be easily checked that by our definition of $\tilde{\mathbf{v}}^{SF}$, we have $\mathbf{u}^{SF} \in \mathcal{A}$. Furthermore, $\mathbf{u}^{SF}$ is constructed to have small stray field (see Sec. 3.4).

Localization of the stray field. Note that our constructions are such that

$$\nabla \cdot \mathbf{u}^{AF} \;+\; \nabla \cdot \tilde{\mathbf{v}}^{AF} = 0 \qquad\qquad \text{and} \qquad\qquad \nabla \cdot \mathbf{u}^{SF} \;+\; \nabla \cdot \tilde{\mathbf{v}}^{SF} = 0, \tag{3.42}$$

in $\mathbb{R} \times \mathrm{T}$. We will use this information to localize the estimates for the stray field energy (for the original idea in the context of ferromagnets, see [6]). Let us note that for every vector field $\mathbf{u}$ and its stray field $\mathbf{v}$ (in the sense of (2.17)), we have

$$\int_{\mathbb{R}\times\mathrm{T}} |\mathbf{v}|^2 \;=\; \inf_{\tilde{\mathbf{v}}} \int_{\mathbb{R}\times\mathrm{T}} |\tilde{\mathbf{v}}|^2, \tag{3.43}$$

where the infimum is taken over all fields $\tilde{\mathbf{v}} \in L^2(\mathbb{R}^3;\mathbb{R}^3)$ satisfying

$$\nabla \cdot \tilde{\mathbf{v}} + \nabla \cdot \mathbf{u} \;=\; 0 \tag{3.44}$$

distributionally. This motivates to define for any $\mathbf{u} \in \mathcal{A}$ and for any $\tilde{\mathbf{v}} \in L^2(\mathbb{R}\times\mathrm{T};\mathbb{R}^3)$, the energy

$$\tilde{E}[\mathbf{u},\tilde{\mathbf{v}}] = \varepsilon \int_\Omega |\nabla u_1^\delta| + Q \int_\Omega |\mathbf{u}_\perp|^2 + \int_{\mathbb{R}\times\mathrm{T}} |\tilde{\mathbf{v}}|^2. \tag{3.45}$$

Hence we have $E[\mathbf{u}] \;\le\; \tilde{E}[\mathbf{u},\tilde{\mathbf{v}}]$, whenever $\tilde{\mathbf{v}}$ satisfies (3.44). In view of (3.42) it then follows that

$$E[\mathbf{u}^{AF}] \;\le\; \tilde{E}[\mathbf{u}^{AF},\tilde{\mathbf{v}}^{AF}], \qquad\qquad E[\mathbf{u}^{SF}] \;\le\; \tilde{E}[\mathbf{u}^{SF},\tilde{\mathbf{v}}^{SF}]. \tag{3.46}$$

The advantage of the quantity $\tilde{E}$ is that it is local in both of its parameters. We hence define the restriction of $\tilde{E}$ on any set $A \subseteq \mathbb{R}\times\mathrm{T}$ by

$$\tilde{E}_{|A}[\mathbf{u},\tilde{\mathbf{v}}] = \varepsilon \int_{A\cap\Omega} |\nabla u_1| + Q \int_{A\cap\Omega} |\mathbf{u}_\perp|^2 + \int_A |\tilde{\mathbf{v}}|^2.$$

3.4 Estimates

In this section, we give the estimates corresponding to the branched needle construction described in the previous section, thus completing the proof of Proposition 3.7. We will show that

Lemma 3.8 (Needles)**.** *For $\gamma^{\frac{1}{3}}\varepsilon^{\frac{2}{3}}|\ln\varepsilon|^{\frac{1}{3}} \lesssim \lambda \lesssim \gamma^2|\ln\lambda|^2$, we have*

$$\frac{1}{\ell^2} \inf_{\mathbf{u}\in\mathcal{A}} E[\mathbf{u}] \;\lesssim\; \gamma^{\frac{1}{3}}\varepsilon^{\frac{2}{3}}\lambda|\ln\lambda|^{\frac{1}{3}}. \tag{3.47}$$

In view of (3.46), it is enough to give the estimate (3.47) in terms of the localized energy $\tilde{E}$, defined in (3.45), using the approximate stray fields $\tilde{\mathbf{v}}^{AF}$ and $\tilde{\mathbf{v}}^{SF}$ defined in the previous section. Before giving the proof of Lemma 3.8, we estimate the restriction of $\tilde{E}$ onto a single transition or closure domain cell. We note that as long as h_0 is bounded away from 1, the estimates for the core cells trivially result in the same upper bounds as for the transition cells. Therefore, in the following we do not include explicit arguments for the core cells.

We first give the estimates for $\mathbf{u}^{AF}$:

Lemma 3.9 (Energy of a transition cell for $\mathbf{u}^{AF}$)**.** *Consider a transition cell Z_{trns} with height h and maximum needle radius r. Suppose that the needle is slender, in the sense of $r \ll h$. Then*

$$\tilde{E}_{|Z_{\mathrm{trns}}}[\mathbf{u}^{AF}, \tilde{\mathbf{v}}^{AF}] \;\lesssim\; \varepsilon r h + \frac{r^4 |\ln \lambda|}{h},$$

where $\mathbf{u}^{AF}$ is defined in (3.32) *and $\tilde{\mathbf{v}}^{AF}$ is given by* (3.33)*.*

Proof. By the definition of $\mathbf{u}^{AF}$, we immediately get the following estimate for the surface energy,

$$\varepsilon \int_{Z_{\mathrm{trns}}} |\nabla u_1^{\delta, AF}| \;\sim\; \int_{Z_{\mathrm{trns}}} |\nabla \chi| \;\lesssim\; \varepsilon r h,$$

where we used the assumption $r \ll h$. It remains to give the estimate for the stray field part of the energy. In view of (3.32), we get

$$\nabla \cdot \mathbf{u}^{AF} \overset{(3.32)}{=} \partial_1 u_1^{AF} \;=\; -2 \sum_{i=1}^{9} \delta(\rho_i(x_1) - |x_\perp - x_\perp^{(i)}|) \partial_1 \rho_i(x_1), \tag{3.48}$$

where δ is the Dirac δ–function. We expect a logarithmic blow–up near each of the needles. This motivates to decompose φ, defined in (3.33), by $\varphi \;=\; \varphi^{(0)} + \varphi^{(1)}$, where $\varphi^{(0)}$ is given by

$$\varphi^{(0)}(x_1, x_\perp) \;=\; \sum_{i=1}^{9} 2\rho_i(x_1)\; \partial_1 \rho_i(x_1) H\big(|x_\perp^{(i)} - x_\perp| - \rho_i(x_1)\big) \ln \frac{\rho_i(x_1)}{|x_\perp - x_\perp^{(i)}|} \tag{3.49}$$

and where, as before, H is the Heaviside function. Let us for the moment assume that the leading order contribution to the stray field energy is due to $\varphi^{(0)}$. In view of (3.49), it is easy to calculate

$$\int_{Z_{\mathrm{trns}}} |\nabla_\perp \varphi^{(0)}|^2 \;\lesssim\; \frac{r^4 |\ln \lambda|}{h} \qquad \text{and} \qquad \int_{Z_{\mathrm{trns}}} |\nabla_\perp \varphi^{(0)}|^4 \;\lesssim\; \frac{r^6}{h^3}. \tag{3.50}$$

We then get

$$\int_{Z_{\mathrm{trns}}} |\tilde{\mathbf{v}}^{AF}|^2 \overset{(3.33)}{=} \int_{Z_{\mathrm{trns}}} |\nabla_\perp \varphi|^2 \;\lesssim\; \int_{Z_{\mathrm{trns}}} |\nabla_\perp \varphi^{(0)}|^2 \overset{(3.50)}{\lesssim} \frac{r^4 |\ln \lambda|}{h}.$$

It remains to check that the energy contribution related to $\varphi^{(1)}$ is of lower order. Indeed, from the definition of φ and $\varphi^{(0)}$ it follows that $\varphi^{(1)}$ satisfies

$$\Delta_\perp \varphi^{(1)} \;=\; 0 \quad \text{in } Z_{\mathrm{trns}} \qquad \text{and} \qquad \partial_{\nu_\perp} \varphi^{(1)} \;=\; -\partial_{\nu_\perp} \varphi^{(0)} \quad \text{on } \partial_\perp Z_{\mathrm{trns}}.$$

In particular, at the boundary of the cell we have

$$|\partial_{\nu_\perp}\varphi^{(1)}| \;\lesssim\; \sum_{i=1}^{9}\frac{\rho_i|\partial_1\rho_i|}{|\rho_i - x_\perp^i|} \overset{(3.29)}{\lesssim} \frac{r^2}{ha} \qquad \text{on } \partial_\perp Z. \tag{3.51}$$

It then follows by standard elliptic estimates that

$$\int_{Z_{\mathrm{trns}}}|\nabla_\perp\varphi^{(1)}|^2 \;\lesssim\; h\int_{\partial_\perp Z_{\mathrm{trans}}}|\partial_{\nu_\perp}\varphi^{(1)}|^2 \overset{(3.51)}{\lesssim} \frac{r^4}{h} \;\ll\; \frac{r^4|\ln\lambda|}{h}.$$

This completes the proof of Lemma 3.9. □

Lemma 3.10 (Energy of a closure domain cell for $\mathbf{u}^{AF}$)**.** *Consider a closure cell Z_{cls} with height h and maximum needle radius r. Suppose that the needle is slender in the sense of $r \ll h$. Then*

$$\tilde{E}_{|Z_{\mathrm{cls}}}[\mathbf{u}^{AF}, \tilde{\mathbf{v}}^{AF}] \;\lesssim\; \varepsilon r h + \frac{r^4|\ln\lambda|}{h} + \lambda r^2 h. \tag{3.52}$$

Proof. The estimate for the energy in the closure domain cells proceeds similarly to that for the transition cells. We decompose $\varphi_1 \;=\; \varphi_1^{(0)} + \varphi_1^{(1)}$, where the function $\varphi^{(0)}$ is given by

$$\varphi_1^{(0)}(x_1, x_\perp) \;=\; 2\rho_{\mathrm{cls}}(x_1)\;\partial_1\rho_{\mathrm{cls}}(x_1)H\big(|x_\perp| - \rho_{\mathrm{cls}}(x_1)\big)\ln\frac{\rho_{\mathrm{cls}}(x_1)}{|x_\perp|}.$$

As in the proof of Lemma 3.9, it can be shown that the contribution of the energy related to $\varphi^{(1)}$ can be neglected. Hence, in the following, we only give the estimates for the functions $\varphi_1^{(0)}$ and φ_2. A straightforward calculation then yields that we have the following bound on the surface energy

$$\varepsilon\int_{Z_{\mathrm{cls}}}|\nabla u_1^{\delta,AF}| \;\lesssim\; \varepsilon r h,$$

where we used the assumption $r \ll h$. Similarly to the arguments in the previous lemma, one can also show that

$$\int_{Z_{\mathrm{cls}}}|\nabla_\perp\varphi_1^{(0)}|^2 \;\lesssim\; \frac{r^4|\ln\lambda|}{h} \qquad \text{and} \qquad \int_{Z_{\mathrm{cls}}}|\nabla_\perp\varphi_1^{(0)}|^4 \;\lesssim\; \frac{r^6}{h^3}. \tag{3.53}$$

Furthermore, from (3.38) and (3.48) we get $|\partial_1\varphi_2| \lesssim \lambda$, and so so

$$\int_{Z_{\mathrm{cls}}}|\partial_1\varphi_2|^2 \;\lesssim\; \lambda r^2 h, \tag{3.54}$$

In view of (3.53) and (3.54), the stray field energy is estimated by

$$\int_{Z_{\mathrm{cls}}}|\tilde{\mathbf{v}}^{AF}|^2 \overset{(3.33)}{\lesssim} \int_{Z_{\mathrm{cls}}}|\nabla_\perp\varphi^{(0)}|^2 + \int_{Z_{\mathrm{cls}}}|\partial_1\varphi_2|^2 \;\lesssim\; \frac{r^4|\ln\lambda|}{h} + \lambda r^2 h. \tag{3.55}$$

This concludes the proof of Lemma 3.10. □

We next give the estimates for $\mathbf{u}^{SF}$:

Lemma 3.11 (Energy of a transition cell for $\mathbf{u}^{SF}$)**.** *Consider a transition cell Z_{trns} with height h and maximum needle radius r. Suppose that the needle is slender, in the sense of $r \ll h$. Then*

$$\tilde{E}_{|Z_{\mathrm{trns}}}[\mathbf{u}^{SF}, \tilde{\mathbf{v}}^{SF}] \lesssim \varepsilon r h + \frac{Q r^4 |\ln \lambda|}{h} + \frac{r^6}{h^3}. \tag{3.56}$$

Proof. We use the notation of the proof of Lemma 3.9, in particular, we decompose $\varphi = \varphi^{(0)} + \varphi^{(1)}$, with $\varphi^{(0)}$ being the dominant term. We first note that by construction $|\nabla_\perp \varphi| \lesssim r/h \ll 1$ (see (3.49)), so $\mathbf{u}^{SF}$ is well-defined in Z_{trns}. Therefore, the surface energy can be estimated as before:

$$\varepsilon \int_{Z_{\mathrm{trns}}} |\nabla u_1^{\delta, SF}| = \varepsilon \int_{Z_{\mathrm{trns}}} |\nabla u_1^{\delta, AF}| \lesssim \varepsilon r h. \tag{3.57}$$

The estimate for the anisotropy energy of $\mathbf{u}^{SF}$ follows from

$$\int_{Z_{\mathrm{trns}}} |\mathbf{u}_\perp^{SF}|^2 \overset{(3.39)}{=} \int_{Z_{\mathrm{trns}}} |\nabla_\perp \varphi|^2 \lesssim \int_{Z_{\mathrm{trns}}} |\nabla_\perp \varphi^{(0)}|^2 \lesssim \frac{r^4 |\ln \lambda|}{h}. \tag{3.58}$$

In order to estimate the stray field energy of $\mathbf{u}^{SF}$, we note that in view of (3.39), we have $|\tilde{\mathbf{v}}^{SF}(x)| \lesssim |\nabla_\perp \varphi(x)|^2$. Hence

$$\int_{Z_{\mathrm{trns}}} |\tilde{\mathbf{v}}^{SF}|^2 \lesssim \int_{Z_{\mathrm{trns}}} |\nabla_\perp \varphi|^4 \lesssim \int_{Z_{\mathrm{trns}}} |\nabla_\perp \varphi^{(0)}|^4 \overset{(3.50)}{\lesssim} \frac{r^6}{h^3}.$$

The above estimates together yield (3.56). □

Lemma 3.12 (Energy of a closure domain cell for $\mathbf{u}^{SF}$)**.** *Consider a closure cell Z_{cls} with height h and maximum needle radius r. Suppose that the needle is slender in the sense of $r \ll h$. Then*

$$\tilde{E}_{|Z_{\mathrm{cls}}}[\mathbf{u}^{SF}, \tilde{\mathbf{v}}^{SF}] \lesssim \varepsilon r h + \frac{Q r^4 |\ln \lambda|}{h} + \frac{r^6}{h^3} + \lambda r^2 h.$$

Proof. As in Lemma 3.11, the function $\mathbf{u}^{SF}$ is well-defined, since $|\nabla_\perp \varphi_1| \lesssim r/h \ll 1$. Using the slenderness condition and the fact that by construction $|\partial_1 \varphi_2| \lesssim \lambda \ll 1$, we again get (3.57). Similarly, (3.58) also holds for the anisotropy energy. Finally, in view of the definitions (3.36), (3.37), (3.38) and (3.41) and in view of (3.53) and (3.54), the stray field energy is estimated by

$$\int_{Z_{\mathrm{cls}}} |\tilde{\mathbf{v}}^{SF}|^2 \lesssim \int_{Z_{\mathrm{cls}}} |\nabla_\perp \varphi_1|^4 + \int_{Z_{\mathrm{cls}}} |\partial_1 \varphi_2|^2 \overset{(3.53),(3.54)}{\lesssim} \frac{r^6}{h^3} + \lambda r^2 h.$$

The above estimates together conclude the proof of Lemma 3.12. □

We are ready to give the proof of Lemma 3.8.

Proof of Lemma 3.8. In view of (3.46), it is enough to give an estimate in terms of the energy $\tilde{E}$ instead of E. As before, consider either a transition or a closure cell Z with dimensions h, a and the maximum needle radius r. The energy of the configurations $\mathbf{u}^{AF}, \tilde{\mathbf{v}}^{AF}$ or $\mathbf{u}^{SF}, \tilde{\mathbf{v}}^{SF}$ are estimated in the previous Lemmas. In the following, we will write $\mathbf{u}, \tilde{\mathbf{v}}$ for a configuration representing either

$\mathbf{u}^{AF}, \tilde{\mathbf{v}}^{AF}$ or $\mathbf{u}^{SF}, \tilde{\mathbf{v}}^{SF}$. Let us for a moment assume that all needles are slender, in the sense of $r \ll h$. In view of Lemmas 3.9–3.12, we then have for any transition cell Z_{trns} and any closure domain cell Z_{cls} with the above dimensions the following estimate:

$$\tilde{E}_{|Z_{\mathrm{trns}}}[\mathbf{u}, \tilde{\mathbf{v}}] \lesssim \varepsilon r h + \frac{\gamma r^4 |\ln \lambda|}{h} + \frac{r^6}{h^3} \quad \text{and} \quad \tilde{E}_{|Z_{\mathrm{cls}}}[\mathbf{u}, \tilde{\mathbf{v}}] \lesssim \varepsilon r h + \frac{\gamma r^4 |\ln \lambda|}{h} + \frac{r^6}{h^3} + \lambda r^2 h. \quad (3.59)$$

Balancing the first two terms in the right-hand sides of (3.59) yields the optimal height for both transition and closure domain cells as a function of the maximum needle radius r:

$$h \;=\; \gamma^{\frac{1}{2}} \varepsilon^{-\frac{1}{2}} r^{\frac{3}{2}} |\ln \lambda|^{\frac{1}{2}}. \quad (3.60)$$

With this choice of h for each cell, the estimates in (3.59) turn into

$$\tilde{E}_{|Z_{\mathrm{trns}}}[\mathbf{u}, \tilde{\mathbf{v}}] \;\lesssim\; \gamma^{\frac{1}{2}} \varepsilon^{\frac{1}{2}} r^{\frac{5}{2}} |\ln \lambda|^{\frac{1}{2}} + \frac{r^6}{h^3} \quad \text{and} \quad \tilde{E}_{|Z_{\mathrm{cls}}}[\mathbf{u}, \tilde{\mathbf{v}}] \;\lesssim\; \gamma^{\frac{1}{2}} \varepsilon^{\frac{1}{2}} r^{\frac{5}{2}} |\ln \lambda|^{\frac{1}{2}} + \frac{r^6}{h^3} + \lambda r^2 h. \quad (3.61)$$

Given any initial height h_1 for the first generation of cells, we use (3.60) to correspondingly choose the width of the first generation of cells. The width of the following generation of cells is inductively defined by (3.22) and (3.60). We terminate the algorithm after M generations of cells as soon as closure domain cells are not too expensive in the sense of

$$\lambda r_M^2 h_M \;\lesssim\; \frac{\gamma r_M^4 |\ln \lambda|}{h_M}. \quad (3.62)$$

We choose the initial height $h_1 = h_1(M)$ such that (3.23) is satisfied, i.e. such that the cells exactly cover Ω. Since in view of (3.22) and (3.60), h_j is a geometric sum, as expected we must have $h_1 \sim 1$ independently of M. In view of (3.60) and (3.62), we then get the following estimate for the needle radius for the first and last generation of cells

$$r_1 \;\sim\; \frac{\varepsilon^{\frac{1}{3}}}{\gamma^{\frac{1}{3}} |\ln \lambda|^{\frac{1}{3}}} \qquad \text{and} \qquad r_M \;\sim\; \frac{\varepsilon}{\lambda}. \quad (3.63)$$

Note that the termination criterion (3.62) is equivalent to $r_M^2/h_M^2 \;\lesssim\; \frac{\lambda}{\gamma |\ln \lambda|}$. Since in view of (3.22) and (3.60) r_j/h_j is monotonically increasing in j, we get

$$\frac{r_j^2}{h_j^2} \;\lesssim\; \frac{\lambda}{\gamma |\ln \lambda|} \qquad \text{for all } 0 \le j \le M. \quad (3.64)$$

Let us assume for the moment that

$$\frac{r_j^6}{h_j^3} \;\lesssim\; \frac{\gamma r_j^4 |\ln \lambda|}{h_j} \qquad \text{for all } 0 \le j \le M. \quad (3.65)$$

In this case, in view of (3.61), the total energy is estimated by

$$\frac{1}{\ell^2} \tilde{E}[\mathbf{u}, \tilde{\mathbf{v}}] \;\lesssim\; \frac{1}{a_1^2} \sum_{j=0}^{\infty} \gamma^{\frac{1}{2}} \varepsilon^{\frac{1}{2}} r_j^{\frac{5}{2}} |\ln \lambda|^{\frac{1}{2}} \overset{(3.63)}{\lesssim} \gamma^{\frac{1}{3}} \varepsilon^{\frac{2}{3}} \lambda |\ln \lambda|^{\frac{1}{3}}.$$

In order to complete the proof, it remains to check the following three consistency criteria.

We first need to verify (3.65). Indeed, (3.65) follows from (3.64) and our second assumption on λ. Secondly, we need to check that our algorithm allows for at least one generation of cells, i.e. $M \gtrsim 1$. In order to see this, we note that $M \gtrsim 1$ is equivalent to $3^M \gtrsim 1$. By our first assumption on λ, we have

$$3^M \overset{(3.22)}{=} \frac{r_1}{r_M} \overset{(3.63)}{\sim} \frac{\lambda}{\gamma^{\frac{1}{3}}\varepsilon^{\frac{2}{3}}|\ln\lambda|^{\frac{1}{3}}} \gtrsim \frac{\lambda}{\gamma^{\frac{1}{3}}\varepsilon^{\frac{2}{3}}|\ln\varepsilon|^{\frac{1}{3}}} \gtrsim 1.$$

Finally, we need to check that the cells are indeed slender in the sense of $r_j \ll h_j$. Indeed, this follows from the second of (3.64), together with the second assumption on λ. This concludes the proof of Lemma 3.8. □

3.5 Constructions for the full energy

In this section, we give the proof of Theorem 3.2. In order to do so, it remains to give a diffuse interface version of the upper constructions in Section 3.3.

We first consider the case of a hard material, i.e. $Q \gtrsim 1$. Hence, we will construct a diffuse interface version $\tilde{\mathbf{u}}^{AF}$ of the magnetization $\mathbf{u}^{AF}$. It is enough to show the construction for a single needle. For simplicity, consider a closure cell Z_{cls} with height h and width a. We recall that for sharp interfaces, we defined $\mathbf{u}^{AF}$ by (3.32), where the shape of the needle is described by the characteristic function χ in (3.30). Now, we define the transition layer

$$\mathcal{S} \;=\; \big\{(x_1,x_\perp) \in Z_{\mathrm{cls}} \;:\; |\,|x_\perp| - \rho_{\mathrm{cls}}(x_1) - d(x_1)\,| \;\leq\; w(x_1)\big\}, \tag{3.66}$$

where the functions $w(x_1)$ and $d(x_1)$ are the thickness and the displacement of the diffuse interface, respectively, given by

$$w(x_1) := \frac{\varepsilon}{Qr}\,\rho_{\mathrm{cls}}(x_1), \qquad d(x_1) := -\rho_{\mathrm{cls}}(x_1)\left(1-\sqrt{1-\tfrac{\varepsilon^2}{3Q^2r^2}}\right). \tag{3.67}$$

We recall that in the present units the quantity εQ^{-1} is just the typical width of Bloch walls, as described in Section 2. We also note that by our assumptions $\varepsilon Q^{-1} \ll r$ and, therefore, $|d(x_1)| \ll w(x_1) \ll \rho_{\mathrm{cls}}(x_1)$, for all $x_1 \in (0,h)$ and all cells. Indeed, by our assumptions $\gamma \gtrsim \lambda^{\frac{1}{2}}|\ln\lambda|^{-1} \gg \lambda$. Therefore, by (3.63) the inequality holds for the closure cell, in which r is the smallest.

Let the "mollification of the Heaviside function" $\tilde{H} \in W^{1,\infty}(\mathbb{R})$ be given by $\tilde{H}(t) = 0$ in $(-\infty,-1]$, $\tilde{H}(t) = \frac{1}{2}(t+1) \in [-1,1]$ and $\tilde{H}(t) = 1$ in $[1,\infty)$. Furthermore let $\tilde{H}_R(t) := \tilde{H}(t/R)$. Analogously to (3.30), we define

$$\tilde{\chi}(x_1,x_\perp) \;:=\; \tilde{H}_{w(x_1)}(\rho_{\mathrm{cls}}(x_1) + d(x_1) - |x_\perp|) \qquad\qquad \text{for } x \in Z_{\mathrm{cls}},$$

We then define $\tilde{\mathbf{u}}^{AF}$ as follows. First we set

$$\tilde{u}_1^{AF} \;=\; \lambda - 2\tilde{\chi}(x) \;\text{ in } Z_{\mathrm{cls}} \qquad\qquad \text{and} \qquad\qquad \mathbf{u}_\perp \;:=\; 0 \;\text{ outside of } \mathcal{S}.$$

Inside the transition layer, we define $\tilde{\mathbf{u}}_\perp^{AF}$, such that $|\tilde{\mathbf{u}}_\perp^{AF}|$ ensures that $\tilde{\mathbf{u}} \in \mathcal{A}$, and that the vectors $\mathbf{e}_1$, $x_\perp$, and $\tilde{\mathbf{u}}_\perp^{AF}$ form a right-handed triplet. A straightforward calculation shows that our choice of $d(x_1)$ ensures charge neutrality on every slice, i.e. $\int_K \tilde{u}_1^{AF}(x_1,x_\perp)\,dx_\perp = 0$ for all $x_1 \in [0,h]$.

In the above construction the exchange and anisotropy energy are supported only in the transition layer $\mathcal{S}$. One easily gets that

$$\int_{\mathcal{S}} \left(\frac{\varepsilon^2}{4Q} |\nabla \tilde{\mathbf{u}}^{AF}|^2 + Q |\tilde{\mathbf{u}}_\perp^{AF}|^2 \right) \lesssim \int_0^h \left(\frac{\varepsilon^2 \rho_{\rm cls}(x_1)}{4Q w(x_1)} + Q \rho_{\rm cls}(x_1) w(x_1) \right) dx_1 \sim \varepsilon r h.$$

In estimating the stray field $\tilde{\mathbf{v}}^{AF}$ of $\tilde{\mathbf{u}}^{AF}$, we can follow the same arguments as for $\mathbf{u}^{AF}$, modifying the definition of $\varphi_1^{(0)}$ to be the radially-symmetric potential due to charges $\nabla \cdot \tilde{\mathbf{u}}^{AF}$ rather than $\nabla \cdot \mathbf{u}^{AF}$. It is easy to see that all the estimates remain unchanged. Comparing the above estimates with those in (3.52), it follows that the localized diffuse interface energy $\mathcal{E}[\tilde{\mathbf{u}}^{AF}, \tilde{\mathbf{v}}^{AF}]$ for a single cell, based on the construction $\tilde{\mathbf{u}}^{AF}$ is not larger in terms of scaling than the localized sharp interface energy $E[\mathbf{u}^{AF}, \tilde{\mathbf{v}}^{AF}]$ of the optimal sharp interface construction in Section 3.3.

The function $\tilde{\mathbf{u}}^{AF}$ can be defined throughout Ω by applying the above construction to every needle in the self-similar geometry described in Section 3.3. The corresponding estimate for $\tilde{\mathbf{u}}^{AF}$ follows. Lastly, we note that the construction in the case of a soft material ($Q \lesssim 1$) proceeds analogously. This concludes the proof of Theorem 3.2.

4 Reduced energy

The analysis of Section 3 provides the scaling of the minimal energy in the limit of thick samples or, correspondingly, when $\varepsilon \to 0$. While the analysis does not require any assumptions about the minimizers (the analysis performed is ansatz-free), the results obtained give only a rough idea about the structure of the minimizers. It seems natural to expect that the minimizers should look like the trial functions used in the construction of the upper bounds. Yet, the precise shape of the domains, as well as the precise constants in the asymptotic behavior of the minimal energy cannot be captured by the analysis above, since it does not address the leading order constant in the scaling of the energy.

In this section, under the assumption that the magnetization is mostly aligned with the easy axis and that the geometry of the minimizers is slender, we derive a reduced sharp interface energy which should provide the leading order behavior of energy for $\varepsilon \ll 1$. Our aim is to reduce energy minimization of E to a two-step process. In the first step, we fix the "shape" of the magnetic domains and construct the energy-minimizing configuration of the magnetization away from the domain walls. In the second step, we minimize the obtained, reduced energy, which depends only on that shape. We note that the heuristic idea of computing the combined contribution of the magnetostatic and anisotropy energies away from the domain walls has been known as the μ^*-method in the physics literature [16, 33]. Below, we assign a precise mathematical meaning to this idea and provide its rigorous justification under specific assumptions. Finally, let us also point out that while in this paper we are interested in the case of applied field near saturation ($\lambda \ll 1$), we expect that the obtained reduced energy to be valid independently of the applied field, even in zero applied field ($\lambda = 1$).

We first introduce the characteristic function χ representing the shape of the domains where the magnetization vector is not aligned with the external field,

$$\chi(x) = 1 \text{ if } m_1(x) < 0, \qquad \chi(x) = 0 \text{ if } m_1(x) \geq 0. \tag{4.1}$$

The reduced energy which is derived in this section is then given by

$$E_0[\chi] = 2\varepsilon \int_\Omega |\nabla \chi| + \gamma \int_{\mathbb{R}\times \mathrm{T}} \partial_1(\lambda\chi_\Omega - 2\chi)(-\Delta_Q^{-1})\partial_1(\lambda\chi_\Omega - 2\chi), \tag{4.2}$$

where the operator Δ_Q is defined by

$$\Delta_Q = \big(\chi_\Omega + \gamma(1-\chi_\Omega)\big)\Delta_\perp + \gamma\partial_1^2,$$

with constant γ defined earlier in (3.1). The admissible class of functions χ for E_0 is

$$\mathcal{A}_0 = \big\{\chi \in BV(\mathbb{R}\times \mathrm{T}; \{0,1\}) : \chi = 0 \text{ in } (\mathbb{R}\times \mathrm{T})\backslash\Omega\big\}.$$

Note that $\Delta_Q \approx \Delta_\perp$ in Ω, when acting on functions that vary slowly in the easy direction, compared to the directions normal to the easy axis. There is a second equivalent formulation for (4.2). Indeed, a straightforward calculation yields that (4.2) can be written as

$$E_0[\chi] = \lambda^2\ell^2 + 2\varepsilon \int_\Omega |\nabla\chi| - 4\lambda\int_\Omega \chi + 4\gamma \int_{\mathbb{R}\times \mathrm{T}} \partial_1\chi(-\Delta_Q^{-1})\partial_1\chi. \tag{4.3}$$

Notice that by lower semicontinuity and coercivity, the minimum of the energy of E_0 is attained in $\mathcal{A}_0$ (see also [6, Theorem 1.2]).

We first note that up to the leading order constant, the reduced energy E_0 has the same scaling of minimal energy as E, i.e., for $\lambda \lesssim \gamma^2|\ln\lambda|^2$ and ℓ sufficiently large we have

$$\frac{1}{\ell^2}\inf_{\chi\in\mathcal{A}_0} E_0[\chi] \;\sim\; \min\left\{\lambda^2, \gamma^{\frac{1}{3}}\varepsilon^{\frac{2}{3}}\lambda|\ln\lambda|^{\frac{1}{3}}\right\}.$$

It can be checked that this result follows by a slight modification of the proof of Theorem 3.1 (replacing u_1 with $\lambda\chi_\Omega - 2\chi$).

In order to show the asymptotic equivalence of the minimum energies for E and E_0, including the leading order constant, we need to make an assumption on the magnetization $\mathbf{m}$. If we assume that the magnetization vector $\mathbf{m}$ does not deviate strongly from the easy axis throughout the sample and, furthermore, that the geometry of the magnetization configuration is slender, we can show that the minimal energies for E_0 and E essentially agree to the leading order:

Theorem 4.1. *Let $\varepsilon \ll 1$ and $\gamma \gg \delta$, where $0 < \delta \ll 1$ is the same as in* (2.16)*. Then*

(i) For every $\mathbf{u} \in \mathcal{A}$ satisfying $|\mathbf{u}_\perp| < \delta$ there exists $\chi \in \mathcal{A}_0$, such that

$$E[\mathbf{u}] \geq (1-\delta^{\frac{1}{2}})E_0[\chi].$$

(ii) For every $\chi \in \mathcal{A}_0$, for which the solution $\tilde\varphi$ of

$$\Delta_Q\tilde\varphi = \gamma\partial_1(\lambda\chi_\Omega - 2\chi). \tag{4.4}$$

satisfies $|\nabla\tilde\varphi| < Q\delta$, there exists $\mathbf{u} \in \mathcal{A}$, such that

$$E_0[\chi] \geq (1-\delta^{\frac{1}{2}})E[\mathbf{u}].$$

Theorem (4.1) is proved at the end of this section via Propositions 4.2 and 4.3. Before giving the proofs for Propositions 4.2 and 4.3, it is instructive to present a formal derivation of E_0 (see also [33]).

We note that both anisotropy and the external field favor alignment of the magnetization with the easy axis. We hence expect that $\mathbf{m} \approx \pm \mathbf{e}_1$ in Ω and should, therefore, have $u_1 \approx \lambda - 2\chi$ there. In view of $|\mathbf{m}| = \chi_\Omega$, this motivates to write $\mathbf{u}$ in Ω in the form

$$\mathbf{u} \;=\; \Big(\lambda - 1 + (1-2\chi)\sqrt{1-|\mathbf{u}_\perp|^2}\Big)\,\mathbf{e}_1 + \mathbf{u}_\perp \;=\; (\lambda - 2\chi)\,\mathbf{e}_1 + \mathbf{u}_\perp + \mathcal{O}(|\mathbf{u}_\perp|^2).$$

For $|\mathbf{m}_\perp| = |\mathbf{u}_\perp| \ll 1$, to the leading order (2.16) then turns formally into

$$E[\mathbf{u}] \simeq 2\varepsilon \int_\Omega |\nabla \chi| + Q \int_\Omega |\mathbf{u}_\perp|^2 + \int_{\mathbb{R}\times \mathrm{T}} |\tilde{\mathbf{v}}|^2. \tag{4.5}$$

Here, the function $\tilde{\mathbf{v}}$ satisfies

$$\tilde{\mathbf{v}} = -\nabla \tilde{\varphi}, \qquad \Delta \tilde{\varphi} = \partial_1(\lambda \chi_\Omega - 2\chi) + \nabla_\perp \cdot \mathbf{u}_\perp \quad \text{in} \quad \mathbb{R}\times \mathrm{T}. \tag{4.6}$$

Following our approach, we minimize (4.5) in two steps. First we take the minimum with respect to $\mathbf{u}_\perp$ with χ fixed. In the second step we minimize the result with respect to all admissible characteristic functions χ. It is not difficult to see (see the proof of Proposition 4.2 for details) that for fixed χ the sum of the last two terms in (4.5) is minimized when

$$\mathbf{u}_\perp = -Q^{-1}\chi_\Omega \nabla_\perp \tilde{\varphi}.$$

Substituting this relation into (4.6), we find that

$$\partial_1^2 \tilde{\varphi} + \Delta_\perp \tilde{\varphi} = \; \partial_1(\lambda\chi_\Omega - 2\chi) + \nabla_\perp \cdot \mathbf{u}_\perp \;=\; \partial_1(\lambda\chi_\Omega - 2\chi) - Q^{-1}\chi_\Omega \Delta_\perp \tilde{\varphi},$$

which is precisely (4.4). Finally, substituting the expression for $\tilde{\varphi}$ in (4.4) into (4.5), it then follows that $E[\mathbf{u}] \simeq E_0[\chi]$, where the reduced energy E_0 is given by (4.2). Here we took into account that Δ_Q is an invertible operator. Thus, to the leading order the energy of minimizers of E_0 should coincide with that of E.

Observe that the reduced energy $E_0[\chi]$ just derived has a form very similar to that of the sharp interface energy E in the case of infinite anisotropy, $Q = \infty$. Indeed, in the latter case the magnetization vector $\mathbf{m}$ is restricted to take only two values in Ω: $\mathbf{m} = \pm \mathbf{e}_1$. For such magnetization configurations the sharp interface energy (2.16) turns into

$$E^{AF}[\mathbf{u}] = \varepsilon \int_\Omega |\nabla u_1^\delta| + \int_{\mathbb{R}\times \mathrm{T}} \partial_1 u_1 (-\Delta^{-1})\, \partial_1 u_1,$$

which coincides with (4.2) for $\gamma = 1$, since in this case $u_1 = \lambda\chi_\Omega - 2\chi$. On the other hand, noting that for slender magnetization configurations we have $-\Delta^{-1} \simeq -\Delta_Q^{-1} \simeq -\Delta_\perp^{-1}$, one should expect

$$E^{AF} \simeq 2\varepsilon \int_\Omega |\nabla_\perp \chi| + \int_{\mathbb{R}\times \mathrm{T}} \partial_1(\lambda\chi_\Omega - 2\chi)(-\Delta_\perp^{-1})\, \partial_1(\lambda\chi_\Omega - 2\chi), \tag{4.7}$$

$$E_0 \simeq 2\varepsilon \int_\Omega |\nabla_\perp \chi| + \gamma \int_{\mathbb{R}\times \mathrm{T}} \partial_1(\lambda\chi_\Omega - 2\chi)(-\Delta_\perp^{-1})\, \partial_1(\lambda\chi_\Omega - 2\chi), \tag{4.8}$$

where χ in (4.7) and (4.8) is given by (4.1). It is easy to see that up to a multiplicative factor the expression in (4.8) coincides with that in (4.7) after rescaling x_2 and x_3 with $\gamma^{-\frac{1}{3}}$. Similarly, the energy per unit area, according to (4.8), is $\gamma^{\frac{1}{3}}$ times the expression in (4.7). Thus, the two energies approximately agree with each other for $Q \gg 1$, and the minimal energy per unit area is smaller by a factor $Q^{\frac{1}{3}}$ for $Q \ll 1$ (see (3.1)). The latter is due to the fact that in this case the *effective* magnetostatic interaction is weakened by a factor of Q, since the stray field is shielded by small deviations of $\mathbf{m}$ from the easy direction, creating magnetic counter-charges. These arguments provide a physical explanation of the apparently surprising fact that the scalings of the energy of non-trivial minimizers both in the case of hard and soft materials agree up to a factor of $Q^{\frac{1}{3}}$ (see also [16, 33]).

We now give a rigorous derivation of the relationship between the reduced energy E_0 and the sharp interface energy E under a few assumptions which appear quite natural physically. Theorem 4.1 is an immediate consequence of the two propositions that follow (for the lower and upper bounds, respectively). We begin with the analysis of the lower bound for $E[\mathbf{u}]$ in terms of $E_0[\chi]$.

Proposition 4.2. *Let $\gamma \gg \delta$, where $0 < \delta \ll 1$ is the same as in (2.16), let $\mathbf{u} \in \mathcal{A}$, and let $|\mathbf{u}_\perp| < \delta$. Then $E[\mathbf{u}] \geq (1 - \delta^{\frac{1}{2}})E_0[\chi]$, where χ is given by (4.1).*

Proof. Let us write $\mathbf{u} = \mathbf{u}^{(0)} + \mathbf{u}^{(1)}$ and $\varphi = \varphi^{(0)} + \varphi^{(1)}$, where φ is defined in (2.17), and

$$\mathbf{u}^{(0)} = \chi_\Omega\{(\lambda - 2\chi)\mathbf{e}_1 - Q^{-1}\nabla_\perp\varphi^{(0)}\}, \qquad \Delta\varphi^{(0)} = \nabla \cdot \mathbf{u}^{(0)}. \tag{4.9}$$

This is always possible, since $\varphi^{(0)}$ is uniquely solvable in terms of χ. Indeed, eliminating $\mathbf{u}^{(0)}$ in the second equation in (4.9) via the first equation in (4.9), one immediately sees that $\varphi^{(0)}$ solves the same equation as $\tilde{\varphi}$ in (4.4). Then, after a straightforward computation, using (2.17) and (4.9), the bulk part of energy $E_{\text{bulk}}[\mathbf{u}] = Q\int_\Omega |\mathbf{u}_\perp|^2 + \int_{\mathbb{R}\times\mathrm{T}} |\nabla\varphi|^2$ can be written as

$$\begin{aligned} E_{\text{bulk}}[\mathbf{u}] &= Q\int_\Omega \left|\mathbf{u}_\perp^{(1)} - Q^{-1}\nabla_\perp\varphi^{(0)}\right|^2 + \int_{\mathbb{R}\times\mathrm{T}} \left|\nabla(\varphi^{(0)} + \varphi^{(1)})\right|^2 \\ &= \int_\Omega \left(Q\left|\mathbf{u}_\perp^{(1)}\right|^2 + Q^{-1}\left|\nabla_\perp\varphi^{(0)}\right|^2 + 2\partial_1\varphi^{(0)}\, u_1^{(1)}\right) + \int_{\mathbb{R}\times\mathrm{T}} \left(\left|\nabla\varphi^{(0)}\right|^2 + \left|\nabla\varphi^{(1)}\right|^2\right). \end{aligned}$$

Using Cauchy-Schwarz inequality, we obtain

$$E_{\text{bulk}}[\mathbf{u}] \geq \int_{\mathbb{R}\times\mathrm{T}} (1 + Q^{-1}\chi_\Omega)|\nabla_\perp\varphi^{(0)}|^2 + \int_{\mathbb{R}\times\mathrm{T}} |\partial_1\varphi^{(0)}|^2 - 2\left(\int_\Omega |\partial_1\varphi^{(0)}|^2 \int_\Omega |u_1^{(1)}|^2\right)^{\frac{1}{2}}. \tag{4.10}$$

Now, recalling (2.15) and (4.1), one can see that in Ω the angle between the vector $\mathbf{m}$ and the vector $m_1^{(0)}\mathbf{e}_1$, where $m_1^{(0)}$ is the first component of the vector $\mathbf{m}^{(0)} = \mathbf{u}^{(0)} + (1 - \lambda)\mathbf{e}_1$, does not exceed $\frac{\pi}{2}$. Note that by (4.9) we have $|m_1^{(0)}| = 1$. Therefore, since $|\mathbf{m}| = 1$ as well, the magnitude of the projection of the vector $\mathbf{u}^{(1)} = \mathbf{m} - \mathbf{m}^{(0)}$ onto $\mathbf{e}_1$ does not exceed 1, and $u_1^{(1)}\mathbf{e}_1$ points in the direction opposite to $m_1^{(0)}\mathbf{e}_1$. From this we conclude that $|u_1^{(1)}| = 1 - \sqrt{1 - |\mathbf{u}_\perp|^2} \leq |\mathbf{u}_\perp|^2$. Therefore, by assumption we have $|u_1^{(1)}| \leq \delta|\mathbf{u}_\perp|$. On the other hand, as can be easily seen, the non-local part of E_0 equals the sum of the first two terms in (4.10). Furthermore, by Cauchy-Schwarz inequality

$$2\left(\int_\Omega \left|\partial_1\varphi^{(0)}\right|^2 \int_\Omega \left|u_1^{(1)}\right|^2\right)^{\frac{1}{2}} \leq 2\left(E_0[\chi]\delta^2 \int_\Omega |\mathbf{u}_\perp|^2\right)^{\frac{1}{2}} \leq 2\delta Q^{-\frac{1}{2}} E_0[\chi]^{\frac{1}{2}} E_0[\mathbf{u}]^{\frac{1}{2}}.$$

Combining the above estimates with the fact that

$$\int_\Omega |\nabla u_1^\delta| = 2(1-\delta^2)\int_\Omega |\nabla \chi|,$$

we arrive at

$$E[\mathbf{u}] \geq 2\varepsilon(1-\delta^2)\int_\Omega |\nabla\chi| + E_{\text{bulk}}[\mathbf{u}] \ \geq (1-\delta^2)E_0[\chi] - 2\delta Q^{-\frac{1}{2}} E^{\frac{1}{2}}[\mathbf{u}]\, E_0^{\frac{1}{2}}[\chi],$$

which yields the statement. □

We next give the proof for the upper bound for $E[\mathbf{u}]$ in terms of $E_0[\chi]$.

Proposition 4.3. *Let $\chi \in \mathcal{A}_0$, let $|\nabla_\perp \tilde{\varphi}| \leq Q\delta$, where $\tilde{\varphi}$ is given by (4.4), for some $0 < \delta \ll \gamma$. Then there exists $\mathbf{u} \in \mathcal{A}$ with $|\mathbf{u}_\perp| \leq \delta$, such that $E_0[\chi] \geq (1-\delta^{\frac{1}{2}})E[\mathbf{u}]$.*

Proof. Set $\varphi^{(0)} = \tilde{\varphi}$ and $\mathbf{u} = \mathbf{u}^{(0)} + \mathbf{u}^{(1)}$, where $\mathbf{u}^{(0)} = \chi_\Omega((\lambda - 2\chi)\mathbf{e}_1 - Q^{-1}\nabla_\perp\varphi^{(0)})$, and $\mathbf{u}^{(1)} = u_1^{(1)}\mathbf{e}_1$ ensures that $|\mathbf{u}^{(0)} + \mathbf{u}^{(1)} + (1-\lambda)\chi_\Omega \mathbf{e}_1| = \chi_\Omega$. Then $\varphi^{(0)}$ solves $\Delta\varphi^{(0)} = \nabla\cdot\mathbf{u}^{(0)}$, and by assumption $|u_1^{(1)}| \leq Q^{-2}|\nabla_\perp\varphi^{(0)}|^2$. The proof is then obtained by retracing the calculation in the proof of Proposition 4.2, noting that in this case $\mathbf{u}_\perp^{(1)} = 0$. We will only need one extra estimate for $\varphi^{(1)}$ solving $\Delta\varphi^{(1)} = \nabla\cdot\mathbf{u}^{(1)}$.

Integrating by parts and applying Cauchy-Schwarz inequality, we obtain

$$\int_{\mathbb{R}\times\mathrm{T}} |\nabla\varphi^{(1)}|^2 = -\int_{\mathbb{R}\times\mathrm{T}} \varphi^{(1)}\Delta\varphi^{(1)} = -\int_{\mathbb{R}\times\mathrm{T}} \varphi^{(1)}\partial_1 u_1^{(1)} = \int_\Omega \partial_1\varphi^{(1)} u_1^{(1)} \leq \left(\int_\Omega |\nabla\varphi^{(1)}|^2 \int_\Omega |u_1^{(1)}|^2\right)^{\frac{1}{2}}.$$

Squaring both sides and using the above estimate for $\left|u_1^{(1)}\right|$, we find that

$$\int_\Omega \left|\nabla\varphi^{(1)}\right|^2 \leq Q^{-2}\delta^2 \int_\Omega \left|\nabla_\perp\varphi^{(0)}\right|^2 \leq \delta^2 Q^{-1} E_0[\chi],$$

which completes the proof. □

5 Transition to non-trivial minimizers

As we showed in Theorem 3.2, there is a change in the scaling behavior of the minimum energy due to appearance of non-trivial minimizers of $\mathcal{E}$ at $\lambda \sim \gamma^{\frac{1}{3}}\varepsilon^{\frac{2}{3}}|\ln\varepsilon|^{\frac{1}{3}}$. In this section we analyze the nature of this transition in more detail. Specifically, we are interested in locating the precise critical value of λ (corresponding to the critical applied field away from saturation) at which this transition occurs. We also address the structure of the domain patterns near the transition point.

As a first step, based on an asymptotic study of the reduced energy E_0, we derive an even further reduced energy E_{00}. We will formally show that near the transition point, in rescaled variables, it is appropriate to consider the energy

$$\bar{E}_{00}[\bar{A}] = \int_0^h \left\{\frac{1}{2\pi}\left(\frac{d\bar{A}}{d\xi}\right)^2 - \bar{A} + \sqrt{\pi\bar{A}}\right\} d\xi, \tag{5.1}$$

where the set of admissible functions is

$$\overline{\mathcal{A}} \;=\; \big\{\bar{A} \in H^1((0,h)) \;:\; \bar{A} \;\geq\; 0,\; \bar{A}(0) = \bar{A}(h) = 0\big\}$$

The function $\bar{A}(\xi)$ is simply the rescaled area of the cross-section of a single needle as a function of the rescaled coordinate along the needle. The single parameter h can be understood as a measure for the effective thickness of the plate. It is defined by

$$h := \frac{\lambda^{\frac{3}{2}}}{\varepsilon\gamma^{\frac{1}{2}} \ln^{\frac{1}{2}}\big(\gamma^{\frac{1}{3}}\varepsilon^{-\frac{1}{3}}\big)}. \tag{5.2}$$

A detailed derivation of the reduced energy $\bar{E}_{00}$ and the precise definition of the quantities $\bar{A}$ and ξ in terms of the original quantities is given in the next subsection.

The advantage of the energy $\bar{E}_{00}$ is that it can be explicitly minimized and its minimizers can be explicitly computed. We identify two critical values, denoted as h_0^* and h_1^*, with $h_0^* < h_1^*$ for the thickness of the rescaled slab, at which transitions in the qualitative behavior of the critical points of $\bar{E}_{00}$ occur. Basically, the result is that the uniform state is the unique global minimizer whenever the effective thickness h of the sample satisfies $h < h_1^*$. Furthermore, the uniform state is even the unique critical point as long as $h < h_0^*$. The precise statement is the following:

Theorem 5.1. *Let $h_0^* = \pi\sqrt{2}$ and let $h_1^* > h_0^*$ be the unique solution of the system of equations*

$$F(\rho_m) = 0 \qquad\qquad \text{and} \qquad\qquad G(\rho_m) = h_1^*, \tag{5.3}$$

where the functions G and F are defined in (5.8) and (5.9), respectively. Depending on the value of h, we then have

1. *If $h < h_0^*$, then $\bar{A} = 0$ is the unique global minimizer of $\bar{E}_{00}$, and there are no other critical points of $\bar{E}_{00}$.*
2. *If $h_0^* \leq h < h_1^*$, then $\bar{A} = 0$ is the unique global minimizer of $\bar{E}_{00}$, but there exist non-trivial critical points of $\bar{E}_{00}$.*
3. *If $h = h_1^*$, then there are two global minimizers, given by $\bar{A} = 0$ and by the unique positive solution of (5.5) vanishing at the endpoints.*
4. *If $h > h_1^*$, then the unique positive solution of (5.5) vanishing at the endpoints is the unique minimizer of $\bar{E}_{00}$.*

Furthermore, the unique positive critical point $\bar{A}_h$ of $\bar{E}_{00}$ obeys $\bar{A}_h(\xi) \sim \xi^{4/3}$ for $h = h_0^*$ and $\bar{A}_h(\xi) \sim \xi$ for $h > h_0^*$.

Thus, the transition from trivial to non-trivial minimizers of $\bar{E}_{00}$ occurs precisely when $h = h_1^*$. Numerically, the critical values of the parameter h are

$$h_0^* \;\approx\; 4.443, \qquad\qquad h_1^* \;\approx\; 6.113.$$

In terms of the original energy $\mathcal{E}$, the statement of Theorem 5.1 has the following interpretation. In view of (5.2), the critical values h_0^* and h_1^* of h define the respective critical values of $\bar{\lambda}$:

$$\bar{\lambda}_0^* = \left(\frac{\gamma {h_0^*}^2}{3}\right)^{\frac{1}{3}}, \qquad \bar{\lambda}_1^* = \left(\frac{\gamma {h_1^*}^2}{3}\right)^{\frac{1}{3}},$$

with the meaning that if one chooses $\lambda = \bar{\lambda}\varepsilon^{\frac{2}{3}}|\ln\varepsilon|^{\frac{1}{3}}$, then the global minimizer of $\mathcal{E}$ will be trivial when $\bar{\lambda} < \bar{\lambda}_1^*$, and non-trivial when $\bar{\lambda} > \bar{\lambda}_1^*$, for fixed $\bar{\lambda}$ and γ as $\varepsilon \to 0$. Similarly, the trivial minimizer is expected to be the unique critical point of $\mathcal{E}$ for $\bar{\lambda} < \bar{\lambda}_0^*$ when $\varepsilon \to 0$. Thus, the transition to non-trivial minimizers for $\varepsilon \ll 1$ is expected to occur at $\lambda = \lambda_1^* \simeq \bar{\lambda}_1^*\varepsilon^{\frac{2}{3}}|\ln\varepsilon|^{\frac{1}{3}}$. We would similarly expect the transition to non-trivial minimizers to occur at this value of λ_1^* in all the energies: E_0, E, and $\mathcal{E}$. We note that λ_1^* can be rigorously shown to give the asymptotic upper bound for the critical value of λ at which non-trivial minimizers emerge by constructing suitable trial functions out of the non-trivial minimizers of $\bar{E}_{00}$. However, since the arguments in this section are based on certain assumptions on the geometry of the magnetic domains, the arguments are not rigorous in terms of a lower bound for λ_1^*.

5.1 Isolated needles

In this section, we present a formal asymptotic derivation of $\bar{E}_{00}$ in (5.1). At the onset of the transition from uniform magnetization to a patterned state as the applied field is reduced it seems natural to expect the appearance of thin slender needle-shaped domains of magnetization opposing the applied field. Under this assumption, it is possible to further reduce the energy E_0 to obtain the precise information about the shape of these domains.

The starting point of the analysis in this section is the reduced energy E_0 in the form of (4.3). We are interested in the magnetization configuration in the form of a single needle. More precisely, we assume that the configuration consists of a a single needle-shaped domain in a sufficiently large sample (i.e. $\ell \gtrsim 1$). In particular, $\operatorname{supp}\chi$ looks like the characteristic function of a prolate ellipsoid of radius $r_0 \ll 1$, extending across Ω in the direction of the easy axis. The crucial observation for the analysis in this section is that due to the slender geometry, the dominant stray field interaction is restricted to slices normal to the easy axis. This interaction, however, is logarithmic and hence does not see the precise shape of the magnetic domains (a similar phenomenon occurs in a related model [26]). In fact, for a domain pattern described above, to the leading order in $r_0 \ll 1$ the Green's function G_Q of the operator $-\Delta_Q$ can be approximated by G_0 given by

$$G_0(\mathbf{r}) = \frac{|\ln r_0|}{2\pi}\,\delta(x_1).$$

Indeed, G_0 gives the leading order behavior of the Green's function for the operator $-\Delta_0 = -\Delta_\perp$. Then the non-local term in the definition of E_0 may be written as

$$\begin{aligned}\int_{\mathbb{R}\times\mathrm{T}} \partial_1\chi(-\Delta_Q^{-1})\partial_1\chi \simeq\ & \frac{|\ln r_0|}{2\pi}\int_0^1\int_{\mathrm{T}}\int_{\mathrm{T}} \partial_1\chi(x_1,\mathbf{r}_\perp)\,\partial_1\chi(x_1,\mathbf{r}'_\perp)\,d^2\mathbf{r}_\perp\,d^2\mathbf{r}'_\perp\,dx_1\\ =\ & \frac{|\ln r_0|}{2\pi}\int_0^1\left(\partial_1\int_{\mathrm{T}}\chi(x_1,\mathbf{r}_\perp)d\mathbf{r}_\perp\right)^2 dx_1.\end{aligned}$$

This motivates to define the function $A:[0,1]\to\mathbb{R}$ by $A(x_1) = \int_{\mathrm{T}}\chi(x_1,\cdot)$, denoting the cross-sectional area of the needle in the slice at x_1. Then (4.3) turns into

$$E_0[\chi]\ \approx \lambda^2\ell^2 + \int_0^1\left(2\varepsilon\int_{\mathrm{T}}|\nabla_\perp\chi|\,d\mathbf{r}_\perp - 4\lambda A + \frac{2\gamma|\ln r_0|}{\pi}|A'|^2\right)dx_1,$$

where we again have used slenderness of the needle in the sense of $\int_\Omega |\nabla\chi| \approx \int_\Omega |\nabla_\perp \chi|$. Minimizing the interfacial contribution of the energy at each x_1 for fixed cross-sectional area then leads to the following expected behaviour for minimizers:

$$\inf_\chi E_0[\chi] \;\approx\; \lambda^2\ell^2 + \inf_A E_{00}[A],$$

where E_{00} is given by

$$E_{00}[A] = \int_0^1 \left(4\varepsilon\sqrt{\pi}\, A^{\frac{1}{2}} - 4\lambda\, A + \frac{2\gamma|\ln r_0|}{\pi}|A'|^2\right)dx_1. \tag{5.4}$$

Note that according to (3.63), at the transition, where $\lambda \sim \gamma^{\frac{1}{3}}\varepsilon^{\frac{2}{3}}|\ln\varepsilon|^{\frac{1}{3}}$, we expect $r_0 \sim \varepsilon^{\frac{1}{3}}\gamma^{-\frac{1}{3}}|\ln\varepsilon|^{-\frac{1}{3}}$ and, hence, $|\ln r_0| \simeq |\ln(\gamma/\varepsilon)^{\frac{1}{3}}|$. Using these two scalings and by introducing the rescaled variables

$$\bar{A} = \frac{\lambda^2}{\varepsilon^2}A, \qquad\qquad \xi = h\, x_1, \qquad\qquad \bar{E}_{00}[A] = \frac{\lambda h}{4\varepsilon^2}E_{00}[\bar{A}],$$

we obtain the energy $\bar{E}_{00}$ in (5.1). Finally, since $\bar{A}(0) > 0$ or $\bar{A}(h) > 0$ imply that there is a charge layer at the plate's surface, causing a lot of stray field energy, to the leading order the minimizers of E_{00} are expected to satisfy $\overline{A}(0) = \overline{A}(h) = 0$.

5.2 Needle shapes and critical fields

In this section, we investigate the minimizers of $\bar{E}_{00}$ and give the proof of Theorem 5.1. We first assume there exists a positive critical point $\bar{A}_h(\xi) \in H_0^1((0,h))$ of $\bar{E}_{00}$, i.e. $A_h > 0$ in $(0,h)$. By standard ODE theory, $\bar{A}_h \in C^2((0,h))$ satisfies the Euler-Lagrange equation for (5.1), i.e.

$$\frac{1}{\pi}\frac{d^2\bar{A}_h}{d\xi^2} = -1 + \frac{\sqrt{\pi}}{2\sqrt{\bar{A}_h}} \qquad\qquad \text{for } \xi \in (0,h). \tag{5.5}$$

Note that (5.5) admits a first integral

$$\frac{1}{2\pi}\left(\frac{d\bar{A}_h}{d\xi}\right)^2 + \bar{A}_h - \sqrt{\pi\bar{A}_h} = \pi C \qquad\qquad \text{for } \xi \in (0,h), \tag{5.6}$$

where $C \in \mathbb{R}$ is an arbitrary constant. Evaluating (5.6) at $\xi = 0$ and in view of $A_h(0) = 0$, we have $C \geq 0$. Evaluating (5.6) at the maximum point of $\bar{A}_h$, yields $\max \bar{A}_h \geq \pi$. We furthermore note that the solution of (5.6) is monotone in $(0, \frac{h}{2})$ and takes its maximum at $\xi = \frac{h}{2}$. It is convenient to introduce the rescaled needle radius $\rho(\xi) = (\bar{A}_h(\xi)/\pi)^{\frac{1}{2}}$ where in view of the above the maximum $\rho_m = \rho(h/2)$ satisfies $\rho_m \geq 1$. Integrating (5.6) over $(0, \frac{h}{2})$, a straightforward calculation yields

$$\frac{h}{2} \;=\; \sqrt{2}\int_0^{\rho_m} \frac{\rho\, d\rho}{\sqrt{C+\rho-\rho^2}} \;=\; \frac{1}{\sqrt{2}}\left(\sec^{-1}(1-2\rho_m) + 2\sqrt{\rho_m(\rho_m-1)}\right). \tag{5.7}$$

Here we used the fact that $C = \rho_m(\rho_m - 1)$, which follows by evaluating (5.6) at $\xi = h/2$. In particular, for any given $h > 0$ a positive critical point of $\bar{E}_{00}$ exists if and only if $h = G(\rho_m)$ for some $\rho_m \geq 1$, where

$$G(\rho_m) \;:=\; \sqrt{2}\left(\sec^{-1}(1-2\rho_m) + 2\sqrt{\rho_m(\rho_m-1)}\right), \tag{5.8}$$

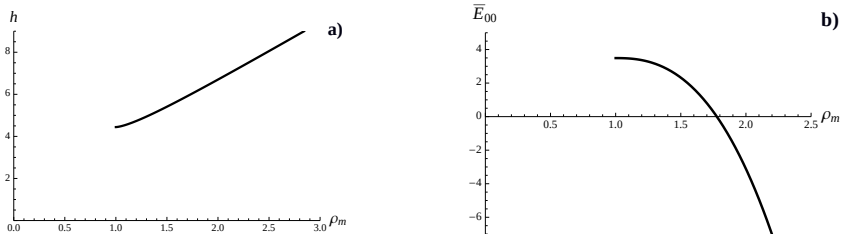

Figure 6: a) Parametric dependence of needle height on the radius, obtained from (5.8). b) Needle energy as a function of radius, obtained from (5.9).

Differentiating (5.8), one gets that $\frac{dG(\rho_m)}{d\rho_m} = \frac{4\sqrt{2\rho_m(\rho_m-1)}}{2\rho_m-1} > 0$, i.e, $G(\rho_m)$ is strictly monotonically increasing for $\rho_m \geq 1$, with $G(1) = \pi\sqrt{2}$ and $G(\rho_m) \to \infty$ as $\rho_m \to \infty$. In particular, a non–trivial critical point of $\bar{E}_{00}$ exists, if and only if $h \geq h_0^* := \pi\sqrt{2}$. Since for every local minimizer the Euler-Lagrange equation holds in every interval of positivity, this also shows that for every $h < h_0^*$, the only critical point of $\bar{E}_{00}$ in $H_0^1((0,h))$ is $\bar{A} = 0$. This completes the proof about the existence or non–existence of non–trivial critical points in (i) and (ii) in Theorem 5.1.

Let us now consider the global minimizers of $\bar{E}_{00}$, which exist, in view of coercivity and lower-semicontinuity of $\bar{E}_{00}$ for all $h > 0$. We first calculate the energy of the needle profile calculated in the first part of the proof. For this, we define

$$F(\rho_m) \;:=\; \bar{E}_{00}[\bar{A}_h] \;=\; \frac{1}{\pi}\int_0^h \left(\frac{d\bar{A}_h}{d\xi}\right)^2 d\xi - \pi h C.$$

An explicit computation then yields

$$F(\rho_m) \;=\; \frac{\pi}{\sqrt{18}}(3 - 4\rho_m(\rho_m-1))\sqrt{\rho_m(\rho_m-1)} + \frac{\pi}{\sqrt{8}}\sec^{-1}(1-2\rho_m). \tag{5.9}$$

Once again, differentiating this function with respect to ρ_m, one gets $\frac{dF(\rho_m)}{d\rho_m} = -\frac{4\pi\sqrt{2\rho_m^3(\rho_m-1)^3}}{2\rho_m-1} < 0$, so that $F(\rho_m)$ is strictly monotonically decreasing for $\rho_m \geq 1$, with $F(1) = \pi^2/(2\sqrt{2})$ and $F \to -\infty$ as $\xi \to \infty$. By monotonicity of G it then follows that $\bar{E}_{00}[\bar{A}_h]$ is strictly decreasing in h for $h \geq h_0^*$. In particular, for $h_1^* > h_0^*$ defined by (5.3), we have $\bar{E}_{00}[\bar{A}_h] > 0$ for $h \in (h_0^*, h_1^*)$ and $\bar{E}_{00}[\bar{A}_h] < 0$ for all $h \in (h_1^*, \infty)$ In particular, for $h \in (0, h_1^*)$, the only global minimizer of $\bar{E}_{00}$ is given by $\bar{A} = 0$. The dependences of h and $\bar{E}_{00}[\bar{A}_h]$ on ρ_m are shown in Fig. 6.

We now claim that for $h > h_1^*$ the global minimizer $\bar{A}$ is unique and is given by $\bar{A} = \bar{A}_h$. Indeed, we first note that $\bar{A}$ is not equal to 0. In view of the above estimates on $\bar{E}_{00}[A_h]$, every interval of positivity contains a point x^* with $\bar{A}(x^*) = \pi$. By strict monotonicity of $\bar{E}_{00}[A_h]$ as a function of h, it is furthermore clear that $\xi = 0$ and $\xi = h$ are boundary points of the intervals of positivity of $\bar{A}$. Suppose that $\bar{A} = 0$ on $I = [\xi_1, \xi_2] \subset\subset (0,h)$ where $\xi_1 \leq \xi_2$. By the above reasoning it follows that there exist points $\xi_1' \in (0, \xi_1)$ and $\xi_2' \in (\xi_2, h)$ such that $\bar{A}(\xi_1') = \bar{A}(\xi_2') = \pi$. It follows that $\tilde{A}$ defined by $\tilde{A} := \pi$ in (ξ_1', ξ_2') and $\tilde{A} := \bar{A}$ outside of (ξ_1', ξ_2') has lower energy than $\bar{A}$ contradicting the assumption that $\bar{A}$ is a minimizer. This shows that $\bar{A} > 0$ in $(0,h)$ and hence $\bar{A} = \bar{A}_h$. This completes the proof of (i)–(iv) in Theorem 5.1.

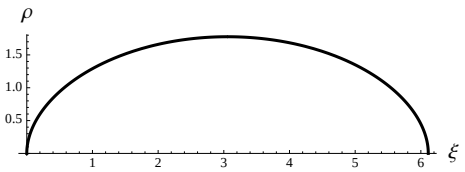

Figure 7: The needle shape at $h = h_1^*$, obtained from (5.5).

In view of (5.6) and (5.7), an explicit calculation yields the following parametric equation for the needle profile for $0 < \xi < \frac{h}{2}$:

$$\begin{aligned}\xi \;=\; & \frac{1}{\sqrt{2}}\left(2\sqrt{(\rho_m-1)\rho_m}+\tan^{-1}\left((2\rho-1)(2\sqrt{(\rho_m-\rho)(\rho_m+\rho-1)})^{-1}\right)\right.\\ & \left.-2\sqrt{(\rho_m-\rho)(\rho_m+\rho-1)}+\cot^{-1}\left(2\sqrt{(\rho_m-1)\rho_m}\right)\right),\end{aligned}$$

see Fig. 7. In particular, one easily checks that for $0 < \xi \ll 1$ the behavior of the radius ρ of the needle near the tip is given by

$$\rho(\xi) \;\sim\; \xi^{\frac{1}{2}} \quad \text{for } h > h_0^* \qquad \text{and} \qquad \rho(\xi) \;\sim\; \xi^{\frac{2}{3}} \quad \text{for } h = h_0^*. \tag{5.10}$$

This concludes the proof of Theorem 5.1.

Acknowledgements

The authors are indebted to R. V. Kohn for pointing out similarities of the considered problem with that arising from models of type-I superconductors, as well as for many valuable discussions. The authors would also like to acknowledge the hospitality of IAM at the University of Bonn, where part of the work was done. C. B. M. was supported, in part, by NSF via grants DMS-0718027 and DMS-0908279.

References

[1] A. Aftalion and S. Serfaty. Lowest Landau level approach in superconductivity for the Abrikosov lattice close to H_{c_2}. *Selecta Math.*, 13:183–202, 2007.

[2] W. F. Brown. Thermal fluctuations of a single-domain particle. *Phys. Rev.*, 130:1677–1686, 1963.

[3] J. A. Cape and G. W. Lehman. Domain nucleation and boundary effects in thin uniaxial plates. *J. Appl. Phys.*, 42:5732–5756, 1971.

[4] R. Choksi. Scaling laws in microphase separation of diblock copolymers. *J. Nonlinear Sci.*, 11:223–236, 2001.

[5] R. Choksi, S. Conti, R. V. Kohn, and F. Otto. Ground state energy scaling laws during the onset and destruction of the intermediate state in a Type-I superconductor. *Comm. Pure Appl. Math.*, 61:595–626, 2008.

[6] R. Choksi and R. V. Kohn. Bounds on the micromagnetic energy of a uniaxial ferromagnet. *Comm. Pure Appl. Math.*, 51:259–289, 1998.

[7] R. Choksi, R. V. Kohn, and F. Otto. Domain branching in uniaxial ferromagnets: a scaling law for the minimum energy. *Commun. Math. Phys.*, 201:61–79, 1999.

[8] R. Choksi, R. V. Kohn, and F. Otto. Energy minimization and flux domain structure in the intermediate state of a Type-I superconductor. *J. Nonlinear Sci.*, 14:119–171, 2004.

[9] R. Choksi, M. A. Peletier, and J. F. Williams. On the phase diagram for microphase separation of diblock copolymers: an approach via a nonlocal Cahn-Hilliard functional. *SIAM J. Appl. Math.*, 69:1712–1738, 2008.

[10] Bernard Dacorogna. *Direct methods in the calculus of variations*, volume 78 of *Applied Mathematical Sciences*. Springer, New York, second edition, 2008.

[11] A. DeSimone, R. V. Kohn, S. Müller, and F. Otto. Magnetic microstructures—a paradigm of multiscale problems. In *ICIAM 99 (Edinburgh)*, pages 175–190. Oxford Univ. Press, 2000.

[12] A. Desimone, R. V. Kohn, S. Müller, and F. Otto. A reduced theory for thin-film micromagnetics. *Comm. Pure Appl. Math.*, 55:1408–1460, 2002.

[13] W. F. Druyvesteyn and J. W. F. Dorleijn. Calculations of some periodic magnetic domain structures; consequences for bubble devices. *Philips Res. Repts.*, 26:11–28, 1971.

[14] L. C. Evans and R. L. Gariepy. *Measure Theory and Fine Properties of Functions*. CRC, Boca Raton, 1992.

[15] M. Gabay and T. Garel. Phase transitions and size effects in the ising dipolar magnet. *J. Phys. France*, 46:5–16, 1985.

[16] A. Hubert and R. Schäfer. *Magnetic domains*. Springer, Berlin, 1998.

[17] J. Kaczér. On the domain structure of uniaxial ferromagnets. *Sov. Phys. – JETP*, 19:1204–1208, 1964.

[18] C. Kittel. Theory of the structure of ferromagnetic domains in films and small particles. *Phys. Rev.*, 70:965–971, 1946.

[19] R. V. Kohn. Energy-driven pattern formation. In *International Congress of Mathematicians. Vol. I*, pages 359–383. Eur. Math. Soc., Zürich, 2007.

[20] R. V. Kohn and S. Müller. Surface energy and microstructure in coherent phase transitions. *Comm. Pure Appl. Math.*, 47:405–435, 1994.

[21] R. V. Kohn and G. Strang. Optimal design and relaxation of variational problems. I. *Comm. Pure Appl. Math.*, 39:113–137, 1986.

[22] C. Kooy and U. Enz. Experimental and theoretical study of the domain configuration in thin layers of $BaFe_{12}O_{19}$. *Philips Res. Repts.*, 15:7–29, 1960.

[23] L. D. Landau and E. M. Lifshits. *Course of Theoretical Physics*, volume 8. Pergamon Press, London, 1984.

[24] L. D. Landau and E. M. Lifshitz. On the theory of the dispersion of magnetic permeability in ferromagnetic bodies. *Phys. Z. Sowjetunion*, 8:153–169, 1935.

[25] E. M. Lifshits and L. P. Pitaevskii. *Course of Theoretical Physics*, volume 8. Pergamon Press, London, 1980.

[26] C. B. Muratov. Droplet phases in non-local Ginzburg-Landau models with Coulomb repulsion in two dimensions. *Comm. Math. Phys.*, (submitted).

[27] F. Otto and T. Viehmann. Domain branching in uniaxial ferromagnets - asymptotic behavior of the energy. *SFB Preprint*, 420, 2008. submitted.

[28] I. A. Privorotskii. Thermodynamic theory of domain structures. *Rep. Prog. Phys.*, 35:115–155, 1972.

[29] R. Prozorov. Equilibrium topology of the intermediate state in type-i superconductors of different shapes. *Phys. Rev. Lett.*, 98:257001, 2007.

[30] R. Prozorov, R. W. Giannetta, A. A. Polyanskii, and G. K. Perkins. Topological hysteresis in the intermediate state of type-i superconductors. *Phys. Rev. B*, 72:212508, 2005.

[31] V. Ya. Shur, E. L. Rumyantsev, E. V. Nikolaeva, and E. I. Shishkin. Formation and evolution of charged domain walls in congruent lithium niobate. *Appl. Phys. Lett.*, 77:3636–3638, 2000.

[32] B. A. Strukov and A. P. Levanyuk. *Ferroelectric Phenomena in Crystals: Physical Foundations*. Springer, New York, 1998.

[33] H. J. Williams, R. M. Bozorth, and W. Shockley. Magnetic domain patterns on single crystals of silicon iron. *Phys. Rev.*, 75:155–178, 1949.